Journal Pre-proofs

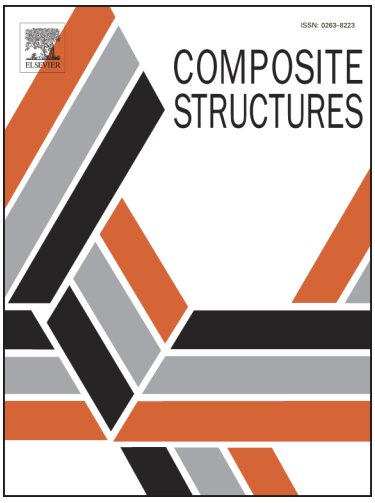

A finite fracture mechanics approach to assess the fatigue life of laminates exhibiting free edge effects

Mohammad Burhan, Zahur Ullah, Zafer Kazancı, Giuseppe Catalanotti

PII: S0263-8223(24)00925-5
DOI: https://doi.org/10.1016/j.compstruct.2024.118797
Reference: COST 118797

To appear in: *Composite Structures*

Received Date: 22 July 2024
Revised Date: 21 November 2024
Accepted Date: 10 December 2024

Please cite this article as: Burhan, M., Ullah, Z., Kazancı, Z., Catalanotti, G., A finite fracture mechanics approach to assess the fatigue life of laminates exhibiting free edge effects, *Composite Structures* (2024), doi: https://doi.org/10.1016/j.compstruct.2024.118797

A Finite Fracture Mechanics approach to assess the fatigue life of laminates exhibiting free edge effects

Mohammad Burhan[1], Zahur Ullah[1,2*], Zafer Kazancı[1], Giuseppe Catalanotti[1,3]†

[1]Advanced Composites Research Group, School of Mechanical and Aerospace Engineering, Queen's University Belfast, Belfast, United Kingdom.

[2]Department of Engineering, Durham University, South Road, Durham, DH1 3LE, UK.

[3]Dipartimento di Ingegneria e Architettura, Università degli Studi di Enna Kore, Cittadella Universitaria, Enna, 94100, Italy.

*zahur.ullah@durham.ac.uk, †giuseppe.catalanotti@unikore.it

Abstract

This study presents the application of a 3D Finite Fracture Mechanics (FFM) criterion for predicting fatigue life estimation of laminates exhibiting free edge effects. The proposed 3D FFM fatigue criterion incorporates interface properties such as the critical interlaminar stress and the incremental energy release rate as functions of the number of cycles. Material constants calibration involves computing critical interlaminar stress using effective stress distribution over an average delamination onset width while assuming a quadratic relation between critical incremental energy release rate and nominal remote maximum stress cycle. The 3D FFM fatigue criterion system of equations consists of two inequalities solved for a unique solution by assuming homothetic crack extension and utilising a non-linear constraint optimisation. The proposed methodology predicts that lower angles of ply orientation in angle-ply laminates exhibit greater finite fatigue life for a given remote cyclic load. Predictions of fatigue life estimation align well with the experimental results from the literature.

Keywords:

Fatigue life assessment, Finite Fracture Mechanics (FFM), Interlaminar stresses, Energy release rate (ERR), Free edge effect.

Nomenclature

a, b	Two semi-axes of a semi-elliptical crack
b_{av}^{c}	Average delamination onset width
E_1,E_2, G_{12},υ_{12}, υ_{23}	Elastic properties of the ply
G	Energy release rate
$\overline{G}$	Total incremental energy release rate
G_c	Interfacial/mixed-mode fracture toughness

$\overline{G}_{max}$	Critical incremental energy release rate at maximum cyclic load
h	Ply thickness
h^o	Nominal ply thickness
$I/II/III$	Three modes of fracture
l^s, l^g, m^s, m^g	Material constants
L	Length of laminate
n	Normalized ply thickness (h/h^o)
N_f	Number of cycles to failure
$N_{f,exp}$	Experimental number of cycles to failure
P_s	Probability of survival
Q_{max}, Q_c	Maximum and critical values of applied load
R	Loading ratio
s	Number of tested specimens for a given stress range
S_x	Interlaminar shear strength for σ_{xz}
t	Total thickness of the laminate
t_{dis}	t-multiplier from the t-distribution
W	Half-width of laminate
x, y, z	Global coordinate system
$(\cdot)^c$	Critical value in static regime
$(\cdot)^f$	Critical value in finite fatigue life regime
$(\cdot)^{\mathrm{H}}$	Homothetic coordinate system
$(\cdot)^l$	Critical value in fatigue limit regime
$\Im$	Tsai's Modulus
α,β	Normalised crack lengths
δ_{max}	Maximum remote cyclic displacement
$\Delta\sigma_o$	Interlaminar shear fatigue limit
$\Delta\sigma_\infty$	Applied remote stress range

ΔG_{th}	Threshold value of energy release rate range
θ	Ply orientation
Λ	Normalised incremental energy release rate
σ_{xz}	Interlaminar shear stress
σ_{∞}	Remote quasi-static stress
σ_{∞}^{c}	Predicted critical static stress
σ^{exp}	Experimental critical static stress
σ_{max}^{∞}	Maximum remote cyclic stress
σ_{xz}^{c}	Critical interlaminar shear stress at maximum cyclic load
ϕ	Polar angle at the semi-elliptical crack front
χ, ψ	Stress function and correction factor
ERR	Energy Release Rate
FEM	Finite Element Method
FFM	Finite Fracture Mechanics
IERR	Incremental Energy Release Rate
VCCT	Virtual Crack Closure Technique

1. Introduction

Composite laminates are crucial materials for applications requiring lightweight design. Their effective properties can be adjusted based on the individual layers' orientation. The mismatch in ply orientation between adjacent layers causes stress singularities at the laminate's free edge, which may lead to interlaminar failure under quasi-static, moisture, fatigue, or thermal loading conditions. This stress concentration, termed the free edge effect, plays a crucial role in aerospace structures. Although interlaminar failure due to the free edge effect has been extensively studied under quasi-static loading conditions, very little has been done to address it under fatigue loading. First identified by Hayashi [1] in the 1960s, the free edge effect phenomenon does not have an exact solution [2]. Therefore, extensive research has been carried out by researchers over the past fifty years to better understand this effect. Building on the initial work of Pipes and Pagano [3], researchers have employed semi-analytical [4,5], closed-form [6–15], and numerical approaches [16–18] to study the free edge effect. Numerous detailed review papers discussing the existing methods and models for the free edge effect can be found in references [2,19–21].

Since the stresses are singular at the free edge [9], traditional local strength of materials criterion is always satisfied. However, Linear Elastic Fracture Mechanics (LEFM) depends on the existence of a flaw to be effective, which limits its use in structures without flaws. An alternative approach is non-local strength-based failure criterion that offers a way to overcome issues arising from singularities by averaging interlaminar stresses over a characteristic/critical length from the free edge. This approach has been implemented by Zhou and Sun [22], Kim and Soni [23], Lagunegrand et al. [24], and Brewer and Lagace [25], drew upon the insights from Whitney and Nuismer [26] in their studies. Another approach involves a fracture mechanics-based criterion, which presumes the presence of a flaw and involves evaluating interfacial energy release rates, as shown in works by Wang and Crossman [27], Leguillon [28], and O'Brien [29]. However, both types of criteria necessitate determining an unknown characteristic/critical length through experimentation beforehand and lack a clearly defined physical meaning. These non-local failure criteria are summarised within the framework of the Theory of Critical Distances (TCD) [30]. In contrast, Leguillon [31] introduced the Finite Fracture Mechanics (FFM) approach, which addresses this issue by formulating a coupled stress and energy criterion. Unlike non-local stress or energy-based approaches, FFM removes the need for priori experimental assessment of the characteristic/critical length, depending only on material intrinsic properties like strength and fracture toughness. FFM has been applied across broad spectrum of structures, involving both singular and non-singular stress raisers. Comprehensive review papers have been covered by Weißgraeber et al. [32] and Doitrand et al. [33] on its theory and application. Additionally, a recent review paper on TCD methods and the FFM approach in the context of delamination of laminates exhibiting free edge effects can be found in [34].

In 2D scenarios, crack extension primarily involves length and direction. However, 3D analysis requires additional assumption to precisely define the shape of the crack front extension, which involves an infinite number of parameters. Leguillon [35] expanded the FFM coupled criterion to 3D using matched asymptotic expansions. García et al. [36] utilised the 3D FFM to analyse the development of transverse cracks in cross-ply laminates, whereas Doitrand et al. [37] implemented it in the study of woven composites for the prediction of critical strain for damage initiation. In their investigation of crack initiation in aluminium-epoxy specimens subjected to four-point bending, Doitrand and Leguillon [38] determined the crack shape using interface normal stress isocontours, depending on a single parameter. Subsequently, they applied this methodology to predict initiation of crack in scarf adhesive joints [39], parameterizing the crack shape based on its surface area. Regarding applications to the free edge effect, Hebel et al. [40], Martin et al. [41], Dölling et al. [5], and Frey et al. [42] utilised FFM to predict the delamination initiation in composite laminates. However, it is noted here that all these FFM models to predict delamination of laminates exhibiting free edge effects are based on a generalised plane strain condition.

It is noteworthy that most of the aforementioned research on the free edge delamination has been performed under quasi-static loading conditions. Little work has been reported on fatigue loading conditions. O'Brien [29] established a power law relation between interfacial energy release rate and delamination growth rates in laminates with free edges under fatigue loading. Later O'Brien [43–45] illustrated that the critical strain energy release rate governed the free edge delamination onset subjected to cyclic loads. An investigation was performed by Scarponi and Barboni [46] involving numerical analysis to determine three-dimensional stress state at free edge under quasi-static loading with the aim to observe the interfaces that are critical and analysing fatigue tests to determine if delamination occurred at expected interfaces. The interlaminar shear stress was utilised by Kim and Crasto [47] to predict the onset of

delamination in conjunction with the SN correlation for in-plane shear. A progressive damage model was developed by Papanikos et al. [48] to predict life of composite laminates subjected to fatigue loading. Stress analysis was performed by three-dimensional Finite Element Method (FEM) model and fatigue failure analysis was conducted by utilising a set of Ye-delamination and Hashin-type failure criterion. Since, fracture in composites due to cyclic loads is one of the prevalent failure mechanisms, the investigation of free edge delamination onset under fatigue loading holds significant importance and therefore should be incorporated into laminate design consideration.

As previously mentioned, the TCD approach depends on a length parameter. This parameter is considered a material property and serves as an input for the TCD model. In contrast, in FFM, the length parameter is a structural parameter that depends also on geometry and is an output to the model. Moreover, TCD breaks down when the structural size approaches or falls below the critical/characteristic length, whereas FFM generally provides improved solutions in such cases. For predicting delamination onset an adequate criterion is required and to the best of authors' knowledge, FFM has not yet been applied to the fatigue loading in the free edge delamination. Therefore, in this paper, a 3D FFM criterion is proposed for predicting delamination of laminates exhibiting free edge effects under fatigue (constant amplitude) loading conditions for a given loading ratio. The two new interface properties (critical stress and incremental energy release rate) in the finite fatigue regime are introduced. These properties are functions of number of cycles to finite fatigue failure and therefore the material constants are estimated using power laws. The system of equations in 3D FFM fatigue fracture criterion is solved by an optimisation problem along with a homothetic crack extension assumption. The symmetric angle-ply laminates are considered, and the predicted finite fatigue life is compared with the experimental results.

This paper is organised as follows. In Section 2.1, the 3D FFM fracture criterion is introduced for static and in Section 2.2 for fatigue limit. Section 2.2 also presents an extension to the finite fatigue regime, followed by the procedures for computation of interface properties in this regime in Section 2.3. The evaluation of a 3D FFM fatigue criterion is then discussed in Section 2.4, along with the finite element models employed in Section 2.5. Results on interlaminar stresses and incremental energy release rates are discussed in Section 3.1. Sections 3.2 and 3.3 are dedicated to the results on interface properties in static and fatigue regimes, respectively. The validation of the 3D FFM criterion and its application for fatigue life estimation are addressed in Section 3.4, followed by the conclusions provided in Section 4.

2. Theory

A four-layer symmetric angle-ply laminate under a remote cyclic load resulting in a maximum cyclic displacement δ_{max} is considered, as illustrated in Fig. 1. Each ply is treated as homogenous, orthotopic, and linear-elastic material with thickness h. The total thickness of the laminate is t, with length $(L \gg h)$, and to ensure that the interlaminar stresses of adjacent edges do not interact, a width of $(2W \geq 16h)$ is considered. The angle θ represents the ply orientation in the angle-ply laminate. The global Cartesian coordinate system is established at the $(-\theta/-\theta)$ interface, centred in the longitudinal direction of the laminate near the free edge, as it is convenient to create the coordinate system at this point due to the singular nature of the stresses. In this setup, the x-axis corresponds to the longitudinal direction, the y-axis to the transverse direction, and the z-axis to the through-the-thickness direction. it is assumed that all interfaces are perfect, ensuring displacement continuity. The resulting reaction forces can be employed to calculate the maximum remote cyclic stress, denoted as σ^{∞}_{max}.

The cracked laminate configuration at the delamination onset under cyclic loading is depicted in Fig. 2. As shown experimentally in [24,25,49] interlaminar delamination onset occurs at the $(\theta/-\theta)$ dissimilar interface in symmetric angle-ply laminates. It is assumed that four identical semi-elliptical delaminations, with semi-axes a and b and polar angle $0^{\circ} < \phi < 180^{\circ}$, originate at these $(\theta/-\theta)$ dissimilar interfaces near the laminate's free edge.

It is important to note here that if a symmetrical laminate is stacked back-to-back, meaning the same sequence of layers is stacked on top of itself, so that the total laminate thickness increases while the ply thickness remains constant. The distribution of interlaminar stress components at any interface remains unchanged, or is zero at the interfaces between sub-laminates, because they are self-equilibrating. As a result, the failure load of back-to-back symmetrical laminates remain same, regardless of the number of stackings, as demonstrated by Lagace et al. [50]. Therefore, ply thickness is a controlling parameter and not laminate thickness in laminates exhibiting free edge effects. Moreover, if the crack dimensions are small compared to the width of the laminate, as is the case in free-edge delamination, the energy release rate of one crack remain unaffected by the presence of other cracks. Therefore, the values computed can also be utilised if only some of the cracks develop (not necessarily all four, as shown in Fig. 2). This aligns with general observations in experimental mechanics, which indicate that cracks tend to develop in regions where local flaws are present, and there is no expectation of symmetry in crack propagation.

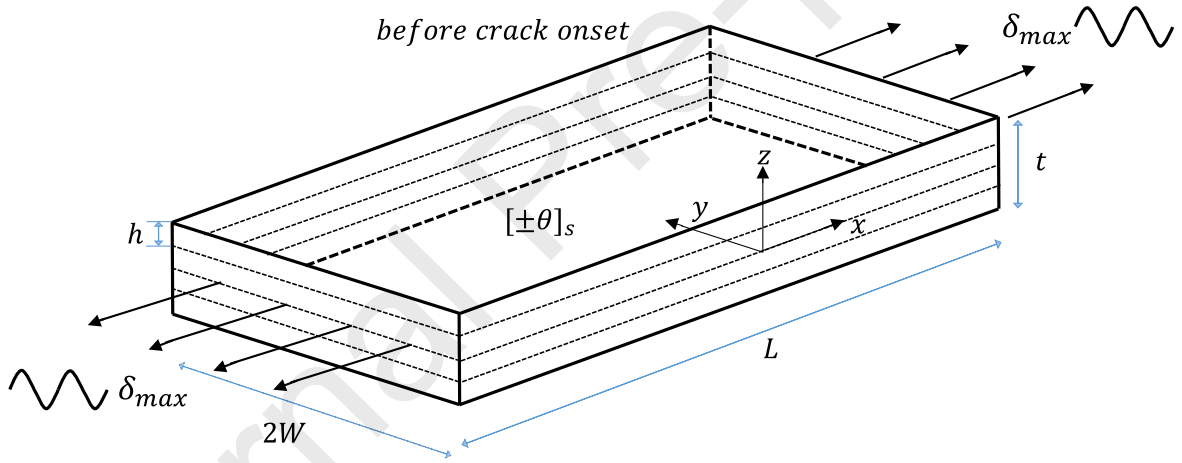

Fig. 1. Symmetric angle-ply laminate with perfect (uncracked) $+\theta/-\theta$ dissimilar interfaces under applied remote cyclic loading.

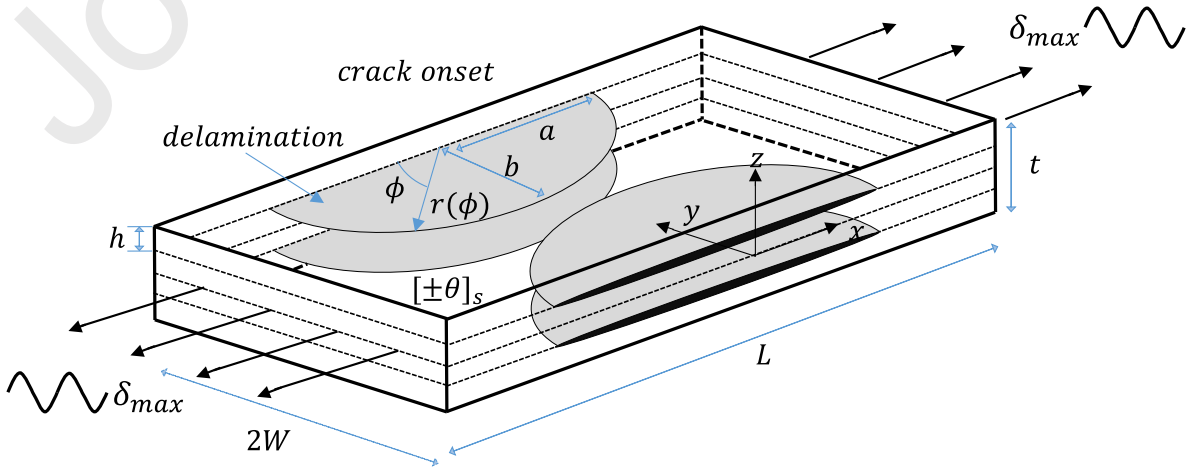

Fig. 2. Symmetric cracked angle-ply laminate with four identical semi-elliptically shaped delaminations located at the $+\theta/-\theta$ dissimilar interfaces under applied remote cyclic loading.

2.1. Finite Fracture Mechanics

FFM fracture criterion, under quasi-static loading, suggests that a crack of finite size forms instantaneously upon initiation if both the stress and energy criteria are simultaneously satisfied. This criterion allows for the prediction of failure load and corresponding unknown finite crack size [31]. In the context of predicting delamination of laminates exhibiting free edge effects in angle-ply laminates, particularly when the interlaminar shear stress σ_{xz} predominates and under consideration of a semi-elliptically shaped crack nucleation, the 3D FFM criterion is given as [51]:

$$\begin{cases} \dfrac{2\sigma_\infty}{\pi ab}\displaystyle\int_{-a}^{a}\int_{0}^{b/a\sqrt{a^2-x^2}} \chi_{xz}\, dy\, dx \geq S_x & (1) \\ \overline{G} = \dfrac{2{\sigma_\infty}^2 h}{\pi ab\Im}\displaystyle\int_{-a}^{a}\int_{0}^{b/a\sqrt{a^2-x^2}} \left({\psi_{II}}^2 + {\psi_{III}}^2\right) dy\, dx \geq G_c & (2) \end{cases}.$$

Here σ_∞ represents the remote quasi-static stress, S_x denotes the interlaminar shear strength for σ_{xz}, G_c signifies mixed mode/interfacial fracture toughness, and $\Im$ represents Tsai's modulus [52], which is computed from 3D stiffness matrix components. The left-hand side of the expression (2) is incremental energy release rate (IERR) $\overline{G}$ and it represents the average differential energy release rate G over the area of finite crack ΔA [32]:

$$\overline{G} = \frac{1}{\Delta A}\int_{0}^{\Delta A} G\, dA\,. \qquad (3)$$

Furthermore, χ_{xz} and ψ_{II}, ψ_{III} represents the normalised interlaminar shear stress and energy release rate in mode II and III, respectively, calculated semi-analytically using FE models and with the following expressions:

$$\sigma_{xz} = \sigma_\infty\, \chi_{xz}$$
$$G_i = \frac{{\sigma_\infty}^2 h}{\Im}{\psi_i}^2 \quad i \in \{II, III\}. \qquad (4)$$

The details of these equations, derived from dimensional analysis, are covered in Ref. [51] and are not reported here for the sake of conciseness. Also, the normalised IERR is denoted by Λ and from the equation (2) is written as:

$$\Lambda = \frac{\overline{G}\Im}{{\sigma_\infty}^2\, h} = \frac{2}{\pi ab}\int_{-a}^{a}\int_{0}^{b/a\sqrt{a^2-x^2}} \left({\psi_{II}}^2 + {\psi_{III}}^2\right) dy\, dx\,. \quad (5)$$

The stress function χ exhibits dependency on material and geometric parameters, whereas ψ is influenced by crack parameters in conjunction with both material and geometric aspects. It is noted here that ψ_I (mode I) is insignificant in angle-ply laminates compared to ψ_{II} (mode II) and ψ_{III} (mode III) and therefore is not considered [51]. The equation (1) represents a stress condition that requires the interlaminar stress, averaged over the potential semi-elliptical crack, must exceed the corresponding interlaminar strength of the material to induce fracture initiation. The equation (2) depicts an energy condition, according to which the total energy release rate for the nucleation of a finite semi-elliptical crack must exceed the fracture toughness to initiate fracture.

For a given interfacial strength and fracture toughness, the set of two equations ((1), (2)) has three unknowns (σ_∞^c, a^c, b^c) representing the critical state. Therefore, the system is underdetermined, and infinite many solutions exist. Moreover, system of equations ((1), (2)) presents an issue in determining the evolving shape and dimensions of the delamination as it extends, given that a semi-elliptical crack involves two dimensions. To address this challenge, Burhan et al. [51] proposed a homothetic approach to crack extension, where the crack shape stays consistent during extension, ensuring a constant aspect ratio a/b. Furthermore, an additional inequality is asserted to ensure that the actual fracture load is minimised among all predicted loads. These adjustments serve to transform the set of equations ((1), (2)) into a uniquely solvable problem, approached as a constrained optimisation problem.

2.2. Fatigue loading

Sapora et al.[53,54] proposed the FFM criterion for estimation of fatigue limit of notches. A similar extension of current 3D FFM static criterion ((1), (2)) to estimate fatigue limit of angle-ply laminates with free edge effect can be written as:

$$\begin{cases} \dfrac{2\Delta\sigma_\infty}{\pi ab}\displaystyle\int_{-a}^{a}\int_{0}^{b/a\sqrt{a^2-x^2}} \chi_{xz}\; dy\, dx = \Delta\sigma_o \\ \dfrac{2\Delta{\sigma_\infty}^2\, h}{\pi ab\Im}\displaystyle\int_{-a}^{a}\int_{0}^{b/a\sqrt{a^2-x^2}} \left({\psi_{II}}^2 + {\psi_{III}}^2\right)\; dy\, dx = \Delta G_{th} \end{cases}, \quad (6)$$

where $\Delta\sigma_o$ and ΔG_{th} are the two material properties that represent interlaminar shear fatigue limit and threshold value of ERR range respectively. Also, $\Delta\sigma_\infty$ signifies the applied remote stress range. Again Eq.(6), like its static counterparts has three unknown variables, fatigue limit $\Delta\sigma_\infty^l$ and crack nucleation dimensions (a^l, b^l), that represents the critical state. Note, both properties ($\Delta\sigma_o$, ΔG_{th}) refer to same load ratio R.

Similar to static and fatigue limit cases, where interface properties (S_x,G_c) and ($\Delta\sigma_o$, ΔG_{th}) are required for the FFM criterion, the finite fatigue life regime existing between these two limit

cases necessitates the introduction of two new interface properties. These are denoted as σ_{xz}^{c} and $\overline{G}_{max}$, representing the critical interlaminar shear stress and IERR at maximum cyclic load, respectively. Implementing these two properties in system of equations ((1), (2)), for a given maximum remote cyclic stress σ_{max}^{∞}, the 3D FFM criterion for the fatigue life estimation in angle-ply laminate is written as:

$$\begin{cases} \dfrac{2\sigma_{max}^{\infty}}{\pi ab}\displaystyle\int_{-a}^{a}\int_{0}^{b/a\sqrt{a^2-x^2}} \chi_{xz}\ dy\ dx \geq \sigma_{xy}^{c} = \sigma_{xy}^{c}(N) \\ \dfrac{2(\sigma_{max}^{\infty})^2 h}{\pi ab\Im}\displaystyle\int_{-a}^{a}\int_{0}^{b/a\sqrt{a^2-x^2}} \left(\psi_{II}{}^2 + \psi_{III}{}^2\right)\ dy\ dx \geq \overline{G}_{max} = \overline{G}_{max}(N) \end{cases}, \quad (7)$$

where N represents number of cycles. A similar extension of the FFM criterion to estimate fatigue life in notched components is proposed by Mirzaei et al. [55].

The interlaminar shear stress σ_{xz} at the dissimilar interface is the critical component for fracture in angle-ply laminates and therefore Kim and Crasto [47] used it in conjunction with power law relation for in-plane shear to predict free edge delamination onset under fatigue loading. On the other hand, a power law relation on N is utilized in Ref. [56] for calculation of ERR at the fatigue delamination onset in End Notched Flexure (ENF) specimens. Therefore, Wohler's curve can be utilised to represent the functions σ_{xz}^{c} and $\overline{G}_{max}$ as a variation with N until finite fatigue failure as:

$$\begin{aligned} \sigma_{xz}^{c} &= \sigma_{xz}^{c}(N) = l^s\, N^{-m^s} \\ \overline{G}_{max} &= \overline{G}_{max}(N) = l^g\, N^{-m^g} \end{aligned}, \quad (8)$$

where material constants l^s, l^g, m^s, m^g are positive numbers and are determined by least-square regression analysis of experimental data (with probability of survival, P_s, equal to 50%) [57].

Once the interface properties (σ_{xz}^{c}, $\overline{G}_{max}$) in finite fatigue regime are known, by using Eq.(8), Eq.(7) is written as:

$$\begin{cases} \dfrac{2\sigma_{max}^{\infty}}{\pi ab}\displaystyle\int_{-a}^{a}\int_{0}^{b/a\sqrt{a^2-x^2}} \chi_{xz}\ dy\ dx \geq l^s\, N^{-m^s} \\ \dfrac{2(\sigma_{max}^{\infty})^2 h}{\pi ab\Im}\displaystyle\int_{-a}^{a}\int_{0}^{b/a\sqrt{a^2-x^2}} \left(\psi_{II}{}^2 + \psi_{III}{}^2\right)\ dy\ dx \geq l^g\, N^{-l^g} \end{cases}. \quad (9)$$

The system of equations (9) above represents the 3D FFM criterion for the finite fatigue life evaluation of angle-ply laminates, for a given material system and load ratio.

The interface properties (σ_{xz}^{c}, $\overline{G}_{max}$) within the finite fatigue regime, like their counterpart in static loading (interlaminar shear strength S_x, and fracture toughness G_c), are generally unknown. This is because these properties are influenced by fibre, matrix material, and ply orientation [58,59]. Furthermore, for a given σ_{max}^{∞}, set of equations (9) is indeterminate with three unknown variables: the critical number of cycles to finite fatigue fracture N_f, and its corresponding finite crack initiation area (represented by a^f and b^f).

The following sections are devoted to address the calculation of interface properties (fatigue regime) and solution of the indeterminate FFM fatigue criterion.

2.3. Computation of interface properties in the fatigue regime

As delamination onset in angle-ply laminates is solely attributed to interlaminar shear loading, the stress-life (SN) curve should be generated specifically for interlaminar shear stress [47]. In structures where singularities exist (e.g., notches, free edges), an averaging approach is often implemented to compute the effective stress to be used in the SN curve method [60].

In recent years, the Theory of Critical Distances (TCD), initially introduced in [61] and subsequently reviewed in [30] has been firmly established as a means of an averaging method in a certain length for evaluating fracture in various materials under quasi-static and fatigue loading conditions. Typically, the length scale considered in laminates with free edge effects subjected to static loading is single [23] or [62] double ply thickness for effective stress computation.

In the present investigation, since the interface property in fatigue regime (σ_{xz}^{c}) is not known, the length scale for its calculation using effective interlaminar stress is assumed as the average of the delamination onset width b_{av}^{c} (which is an output computed from the 3D FFM static criterion as outlined in set of equations ((1), (2))), across the laminate configurations taken under consideration subjected to fatigue loading. This approach eliminates the ambiguity of using a single or double ply thickness as in TCD, ensuring the length scale is derived from the FFM static model. Therefore, the critical interlaminar shear stress at maximum cyclic load σ_{xz}^{c}, as an interface property, is expressed as the interlaminar shear stress averaged in b_{av}^{c}:

$$\sigma_{xz}^{c} = \frac{1}{b_{av}^{c}} \int_{0}^{b_{av}^{c}} \sigma_{xz}\, dy\,. \qquad (10)$$

Using Eq. (4), σ_{xz}^{c} can be computed for a maximum remote cyclic stress σ_{max}^{∞} as:

$$\sigma_{xz}^{c} = \sigma_{xz}^{c}(N) = \frac{\sigma_{max}^{\infty}}{b_{av}^{c}} \int_{0}^{b_{av}^{c}} \chi_{xz}\, dy\,. \qquad (11)$$

The benchmark case for delamination onset from an initial flaw in Ref. [56], the maximum load Q_{max} is calculated in ENF specimens based on a quadratic relationship between Q_{max} and the energy release rate at maximum load in mode II, G_{IImax}:

$$\frac{G_{IImax}}{G_c} = \left(\frac{Q_{max}}{Q_c}\right)^2, \qquad (12)$$

where G_c and Q_c are critical values of energy release rate in mode II and applied static load, respectively. A similar approach can be followed to calculate the incremental energy release rate at maximum cyclic load $\overline{G}_{max}$, where it is supposed to be a quadratic function of σ^{∞}_{max}. Therefore, $\overline{G}_{max}$ is written as:

$$\overline{G}_{max} = \overline{G}_{max}(N) = G_c\left(\frac{\sigma^{\infty}_{max}}{\sigma^{exp}}\right)^2, \qquad (13)$$

where σ^{exp} is a critical static load known experimentally and mixed mode toughness (G_c) is estimated through an inverse calculation using 3D FFM static criterion proposed in Ref. [51]. The procedure to estimate G_c is outlined in Appendix A.

Upon obtaining the parameters (G_c, b^c_{av}) using 3D FFM static criterion, the interfacial properties ($\overline{G}_{max}(N)$, $\sigma^c_{xz}(N)$) for fatigue regime, using Eq.(11) and (13), can be determined for a different nominal remote maximum stress cycle σ^{∞}_{max} that are related to the experiments. Subsequently, using these interfacial properties under fatigue regime, the material constants (l^s,m^s, l^g, m^g) are computed using Eq.(8) through best-fitting procedure.

2.4. Evaluation of 3D FFM fatigue criterion

Identical to the 3D FFM criterion under static loading, a homothetic crack extension (Section 2.1) is presumed in finite fatigue regime. Furthermore, the evaluation of the critical number of cycles N_f and its corresponding size of finite crack initiation (a^f, b^f) leads to a constrained nonlinear standard optimisation problem.

The 3D FFM fatigue criterion (equations in (9)) can be explicitly written in terms of N as follows:

$$\begin{cases} N \geq \left[\dfrac{2\sigma^{\infty}_{max}}{l^s \pi a b}\displaystyle\int_{-a}^{a}\int_{0}^{b/a\sqrt{a^2-x^2}} \chi_{xz}\, dy\, dx\right]^{-1/m^s} \\ N \geq \left[\dfrac{2(\sigma^{\infty}_{max})^2 h}{l^g \pi a b \Im}\displaystyle\int_{-a}^{a}\int_{0}^{b/a\sqrt{a^2-x^2}} \left(\psi_{II}{}^2 + \psi_{III}{}^2\right)\, dy\, dx\right]^{-1/m^g}. \end{cases} \qquad (14)$$

For the solution of system of equations (14), a standard optimisation technique is utilised. In the numerical implementation process, for a given random value of maximum nominal remote

stress cycle, σ_{max}^{∞}, N_f and a^f, b^f are obtained as solutions to the following constrained nonlinear optimisation problem:

$$N_f = \min_{a,\ b}\left[\max\left\{\left(\frac{\sigma_{max}^{\infty}\, s(\chi_{xz},a,b)}{l^s A}\right)^{-1/m^s}, \left(\frac{(\sigma_{max}^{\infty})^2 h\, g(\psi_i,a,b)}{l^g A \Im}\right)^{-1/m^g}\right\}\right], \quad (15)$$

where $A=\frac{\pi ab}{2}$ represents the area of the semi-ellipse. The functions $s(\chi_{xz},a,b)$ and $g(\psi_i,a,b)$ characterise the stress and energy conditions, respectively, and are defined as:

$$\begin{aligned} s(\chi_{xz},a,b) &= \int_{-a}^{a}\int_{0}^{b/a\sqrt{a^2-x^2}} \chi_{xz}\, dy\, dx \\ g(\psi_i,a,b) &= \int_{-a}^{a}\int_{0}^{b/a\sqrt{a^2-x^2}} \left(\psi_{II}{}^2 + \psi_{III}{}^2\right) dy\, dx, \end{aligned} \quad (16)$$

with the nonlinear equality constraint that the number of cycles to failure from both conditions must be equal:

$$c_{eq}(a,b) = N(\chi_{xz},a,b) - N(\psi_i,a,b) = 0. \quad (17)$$

The procedure yields the minimum number of cycles to failure N_f necessary for nucleating a finite semi-elliptical crack characterising by dimensions a^f and b^f, while ensuring both stress and energy criteria are satisfied. The flowchart in Fig. 3 outlines the steps taken to employ the 3D FFM fatigue criterion for laminates exhibiting free edge effects.

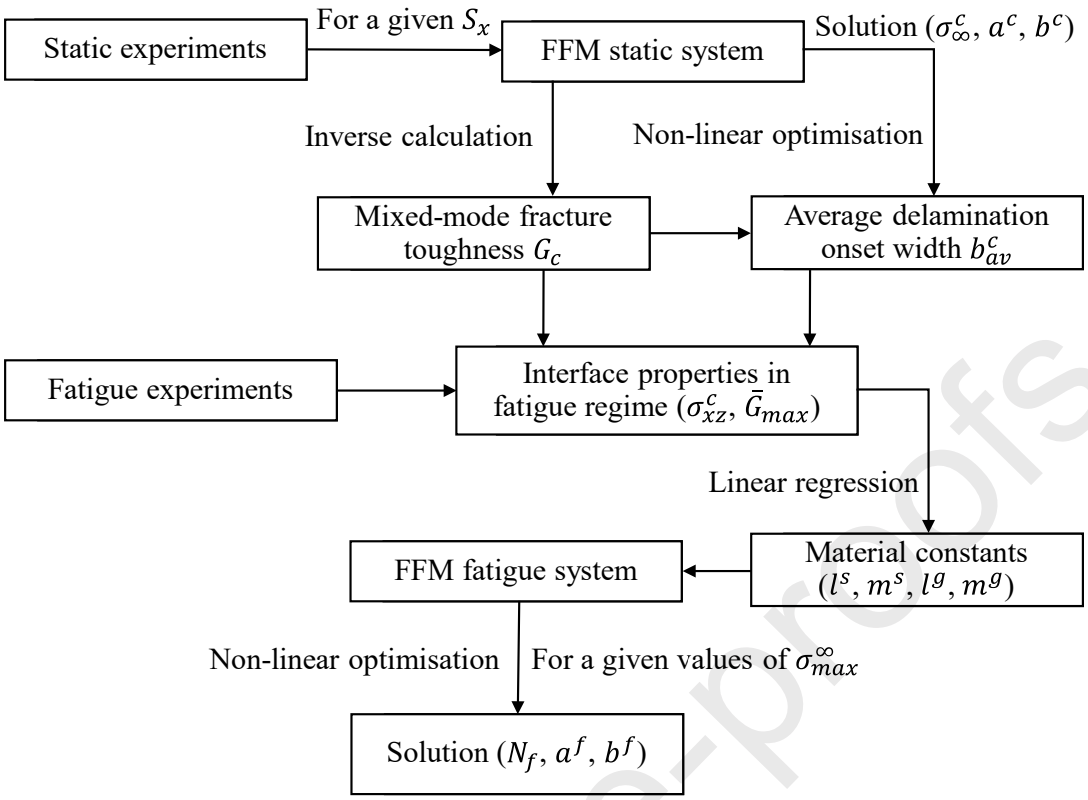

Fig. 3. Flowchart illustrating the step-by-step procedure for applying the 3D FFM fatigue fracture criterion.

2.5. Finite Element models

For both interlaminar stresses and ERR 3D FE models, linear 8-node brick reduced integration elements (C3D8R) are utilised. Full details of the implemented FE models are provided in Ref. [63] and are omitted here to maintain conciseness.

Since $[\pm\theta_n]_s$ laminates are considered which are characterised by only z-axis symmetry. The numerical computation pertaining to interlaminar stresses and energy release rates are conducted utilising half-laminate models ($0 < z < 2h$). The prescribed and symmetry boundary conditions associated to both models are shown in Fig. 4 and Fig. 5, respectively.

A thin resin-rich transition layer, with a thickness of 2% of a single ply, is modelled at the dissimilar interface (see Fig. 4) where the interlaminar stresses are evaluated at Gauss integration points using Abaqus. Further information on incorporation and thickness of this transition layer can be found in Ref. [63]. This transition layer consists of a single through-thickness element, with the Gauss integration point of the element at the free edge located 1.25 % of h from the free edge, ensuring close proximity to the free edge.

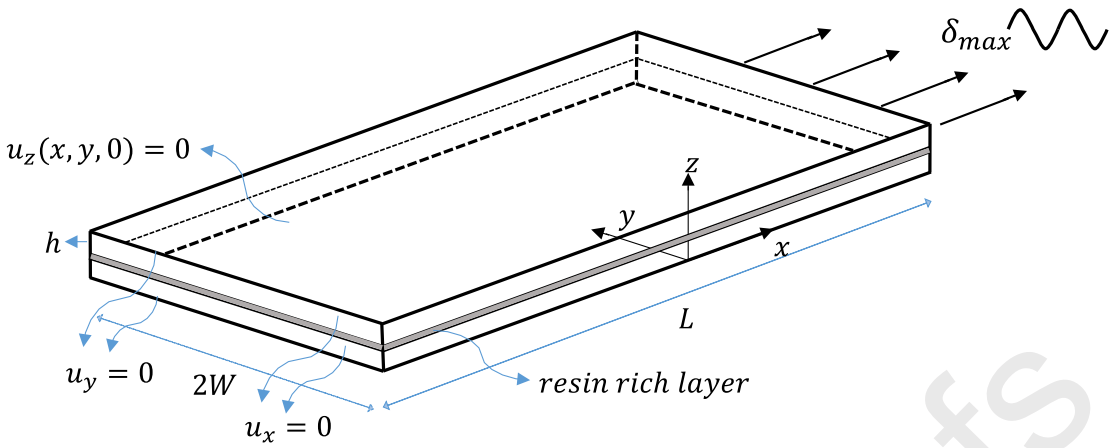

Fig. 4. The prescribed and symmetric boundary conditions of a half-uncracked laminate with resin-rich transition layer at the $(\theta/-\theta)$ dissimilar interface.

Owing to the negligible influence exerted by one crack within the top half laminate ($0 < z < 2$ h) on the stress field of adjacent edge crack situated on the opposite side (as discussed in Section 2), only one crack is considered. This is elucidated in Ref. [51] and its illustration is provided in Fig. 5. The ERR is computed along the crack front employing the 3D Virtual Crack Closure Technique (3D-VCCT) in Abaqus. The relative crack closure length near crack front (ratio of size of element to the semi-elliptical crack perimeter) is maintained 0.02 throughout [63]. Detailed analysis of the element sizes at the semi-elliptical delamination front for the convergence of ERR values using 3D-VCCT is found in Ref. [63].

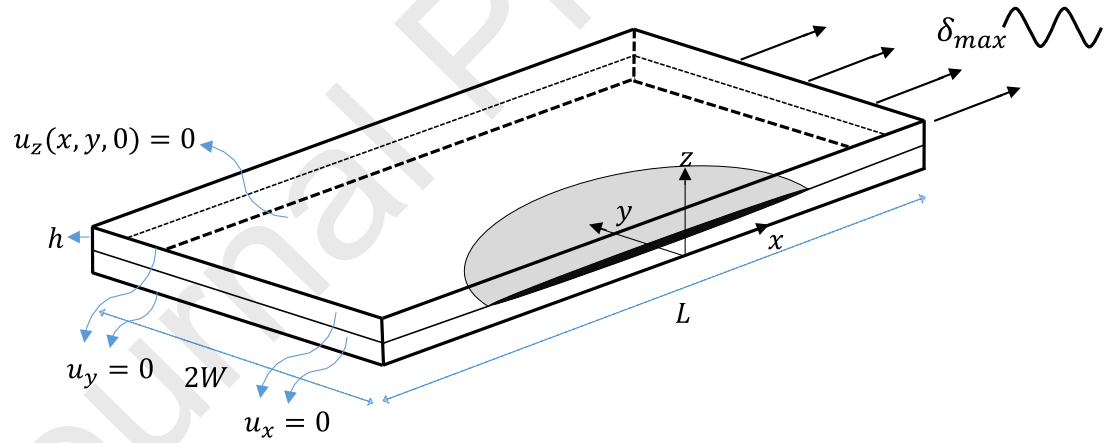

Fig. 5. The prescribed and symmetric boundary conditions of a half-cracked laminate with only one semi-elliptical delamination considered at the $(\theta/-\theta)$ dissimiliar interface.

A typical FE mesh corresponding to both FE models is shown in Fig. 6. For interlaminar stress evaluation (see Fig. 6 (a)), the mesh is refined near the free edge to accurately capture the high-stress gradients and transitions to a coarser mesh toward the interior of the laminate where the stresses rapidly decrease. For ERR calculations (see Fig. 6 (b)), a structured mesh near the semi-elliptical crack front ensures element orthogonality to the crack front, a requirement for accurate VCCT application [64].

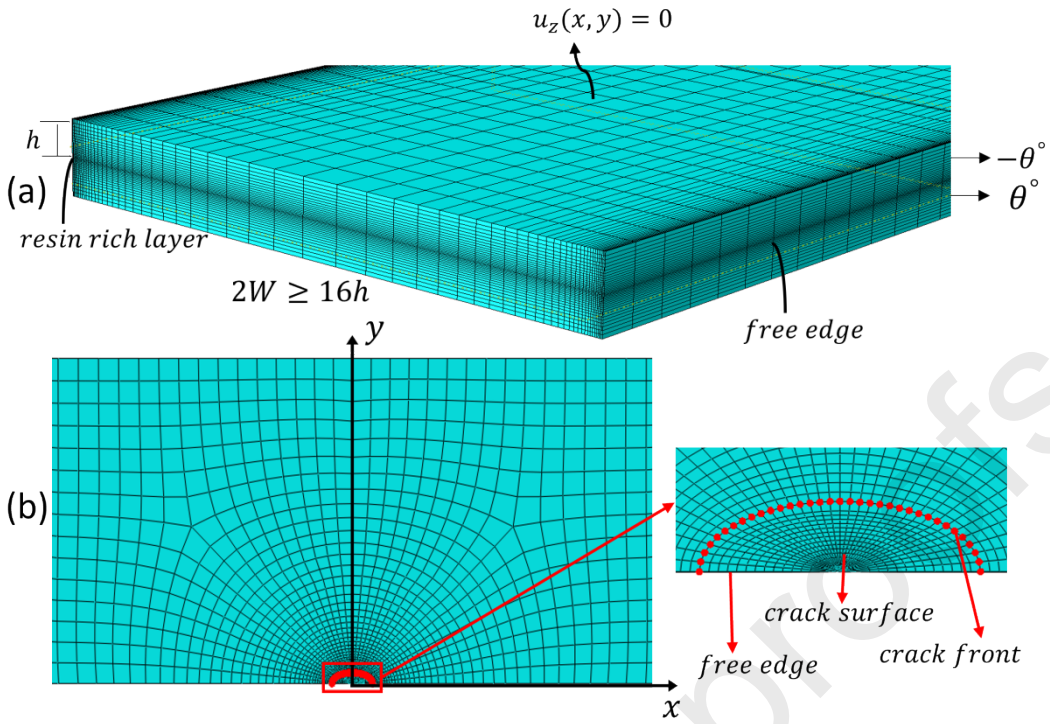

Fig. 6. Typical FE mesh near (a) the free edge for determining interlaminar stresses and (b) a semi-elliptical crack emanating from the free edge for computing ERR.

3. Results and Discussion

In this paper, data is referred to two distinct material systems: carbon/epoxy M79/UD600 and glass/epoxy Scotchply/1003, as detailed in Table 1. The edge delamination experimental findings concerning free edge fracture stresses for angle-ply laminates ($[\pm\theta_n]_s$ of M79/UD600, where θ=10, 20, 30 and n=1, 3) are taken from Ref. [65]. Table 1 includes the elastic properties and nominal ply thickness, h^o, for M79/UD600, also obtained from Ref. [65], along with the interlaminar shear strength, S_x, (acquired from material manufacturer [66]) and Tsai's Modulus, $\Im$, (taken from Ref. [67]). For Scotchply/1003, the experimental data of free edge fracture stresses for angle-ply laminates ($[\pm\theta_2]_s$, where θ=25, 35, 45) under both static and fatigue (tension-tension with loading ratio, R=0.05) loading conditions are taken from Ref. [68]. Table 1 provides h^o for Scotchply/1003 (from Ref. [68]), along with the interlaminar shear strength (from the Ref. [69]) and the elastic properties (from Ref. [70]). Further relevant details of the experimental setups, including schematic representations, are provided in Table 2.

Table 1. Elastic properties, ply thickness, and interlaminar shear strengths of material systems considered.

Material system	E_{11} (GPa)	E_{22}=E_{33} (GPa)	G_{12}=G_{13} (GPa)	G_{23} (GPa)	ν_{12}= ν_{13}	ν_{23}	$\Im$ (GPa)	h^o (mm)	S_x (MPa)
M79/UD600	136.5	10.1	4.1	3.4	0.37	0.5	194	0.617	75

Scotchply/1003	43.2	10	4.49	4.17	0.31	0.44	43.2	0.2125	43

Table 2. Relevant details of the edge delamination test experimental setups.

Test setup	**Edge delamination tests**		
Reference	[65]	[68]	
Loading condition	Quasi-static	Quasi-static	Fatigue
Loading details	-	-	Loading ratio (R=0.05) Frequency=2Hz
Material system	Carbon/epoxy M79/UD600	Glass/epoxy Scotchply/1003	
Layup	$[\pm\theta_n]_s$ (θ=10, 20, 30 and n=1, 3)	$[\pm\theta_2]_s$ (θ=25, 35, 45)	
Specimen details	Curing (autoclave) at 80℃ for 8 hours.	Vacuum operation of laminates for 18 hours at 1.3 Pa absolute pressure. Curing (oven) at 150℃ and 172 kPa for 2 hours.	
Procedure	Zwick 100. Displacement control (2mm/min).	MTS (electro-hydraulic servo-controlled). Load control (1.15 MPa/s)	

Schematic	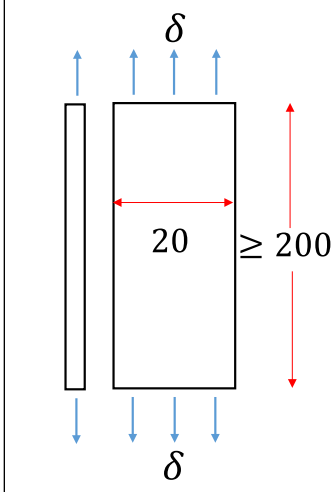	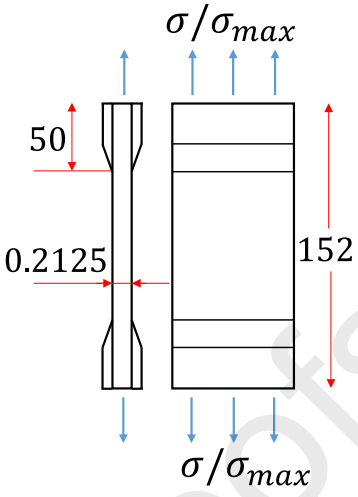

All dimensions in mm

Considering that Ref. [68] experimentally examined free edge effects on tensile strength and fatigue behaviour across laminates of various widths, only experimental data corresponding to widths exceeding four times the total thickness are considered. This ensures that the interlaminar stresses of adjacent edges do not interact. Consequently, this necessitates a re-evaluation of the average experimental fracture stresses under static loading conditions based on the selected data. As Scotchply/1003 constitutes a glass fibre reinforced polymer, Tsai's Modulus is not applicable, and the longitudinal elastic modulus is utilised in this context.

3.1. Interlaminar stresses & incremental energy release rates

This section discusses the interlaminar stresses and incremental energy release rates, which are computed semi-analytically (as mentioned in Sections 2.1 and 2.5), for the selected laminates with different ply orientations. The evaluated normalised interlaminar shear, χ_{xz}, and normal, χ_{zz}, stresses are depicted in Fig. 7 (a) and (b), respectively. The χ_{xz} for M79/UD600 increases with ply orientation as shown in Fig. 7 (a). Although, both χ_{xz} and χ_{zz} functions display a weak singularity in the vicinity of the free edge, their influence diminishes quickly towards the transverse direction of the laminate. The interlaminar shear stress exhibits significant dominance compared to interlaminar normal compressive stress. Hence, only shear stresses are considered for the evaluation of 3D FFM fatigue criterion. Furthermore, since in symmetric angle-ply laminates interlaminar crack initiation originates at the $(+\theta/-\theta)$ dissimilar interface [24,49], only stresses between plies with dissimilar orientations are considered.

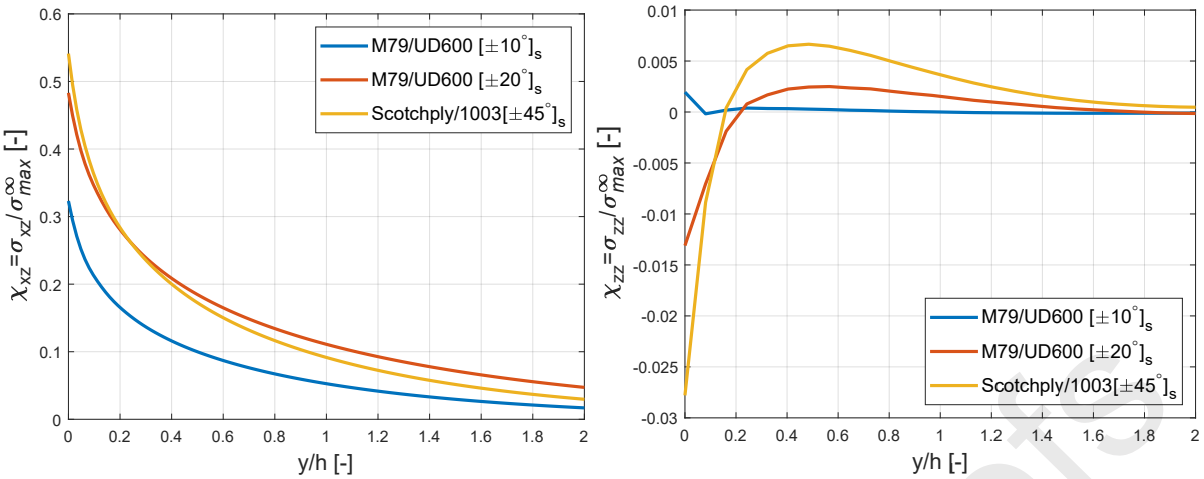

(a) (b)

Fig. 7. Normalised interlaminar (a) shear stress, χ_{xz}, and (b) normal stress, χ_{zz}, for the selected laminates along the $(+\theta/-\theta)$ dissimilar interface.

The normalised IERR Λ for the considered laminates with different ply orientations is shown in Fig. 8, utilising the homothetic coordinate system [51]. In this coordinate system, each point of the domain denotes a potential/possible extension of the delamination (semi-elliptical in shape) via a homothetic path, where the aspect ratio of the crack is kept constant. The axes of this coordinate system are represented by the normalised crack semi-axes with a superscript H, $\alpha^{\mathrm{H}} = a/h$, and $\beta^{\mathrm{H}} = b/h$. The normalised IERR Λ is observed to increase with ply orientation and α^{H}, however decreases slightly at higher values of β^{H}.

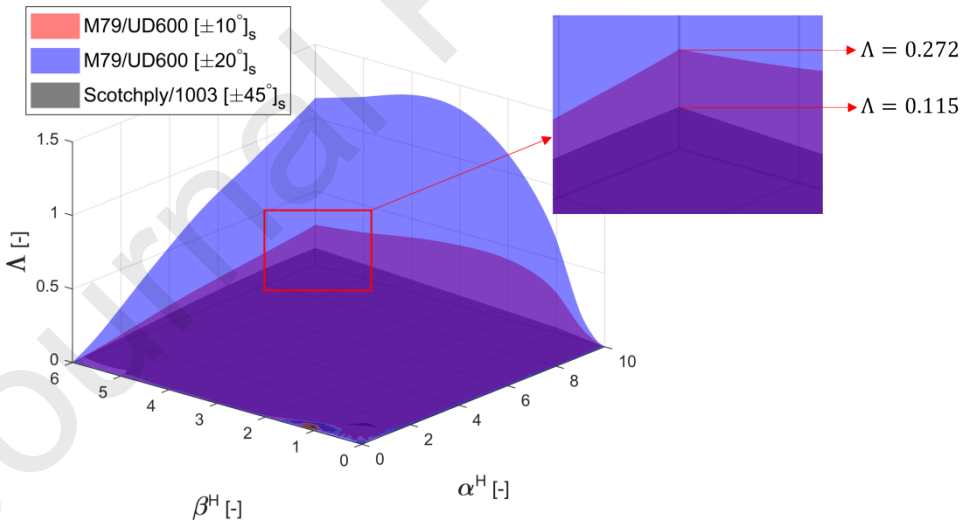

Fig. 8. Normalised IERR Λ with respect to homothetic crack parameters for the considered laminates.

3.2. Fracture toughness and average delamination onset

This section presents the results of mixed-mode fracture toughness and average delamination onset width parameters (G_c, b^c_{av}), which have been computed using 3D FFM static criterion as outlined in Section 2.3. These parameters are evaluated for the selected laminates with different ply orientations. For a given interlaminar shear strengths (Table 1), Fig. 9 (a) and Fig. 10 (a)

illustrates the interface toughness for the M79/UD600 and Scotchply/1003, respectively, alongside corresponding residuals depicted in Fig. 9 (b) and Fig. 10 (b) with respect to the number of iterations. The analysis for M79/UD600 includes assessment of both normalised ply thickness (n=total/nominal ply thickness) and ply orientation, while Scotchply/1003 is assessed only for different ply orientations.

An evident trend shows that interface fracture toughness decreases as both normalised ply thickness and ply orientation increase. Size effects in fracture toughness evaluation are often observed. In fact, these observations are in accordance with several researchers [58,71,72], who have observed a decline in fracture toughness as ply thickness increases, and as highlighted in Ref. [58], with respect to ply orientation as well.

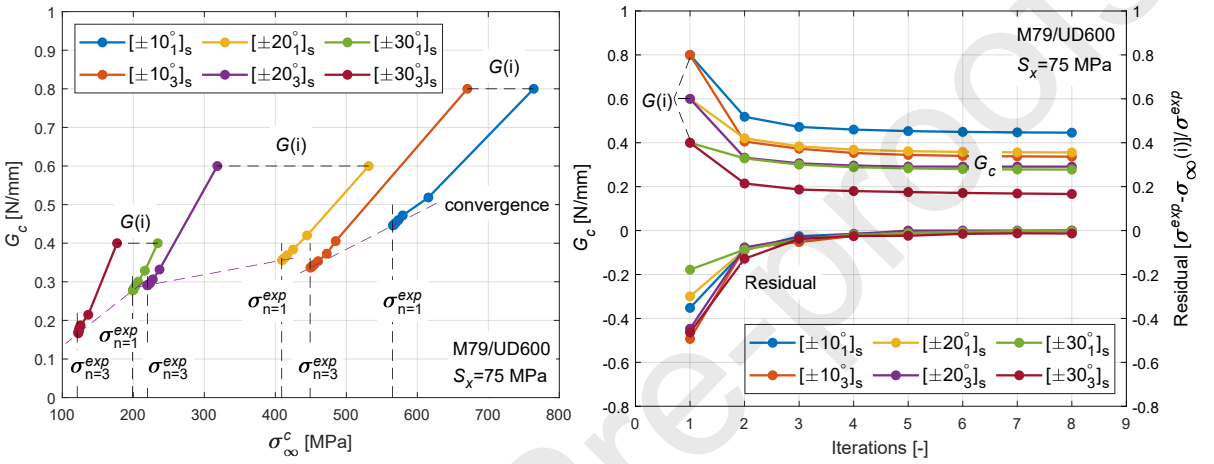

(a) (b)

Fig. 9. Evaluated interfacial fracture toughness for M79/UD600 laminate with respect to (a) experimental failure stress and (b) the corresponding number of iterations, across various ply orientations and normalised effective ply thicknesses.

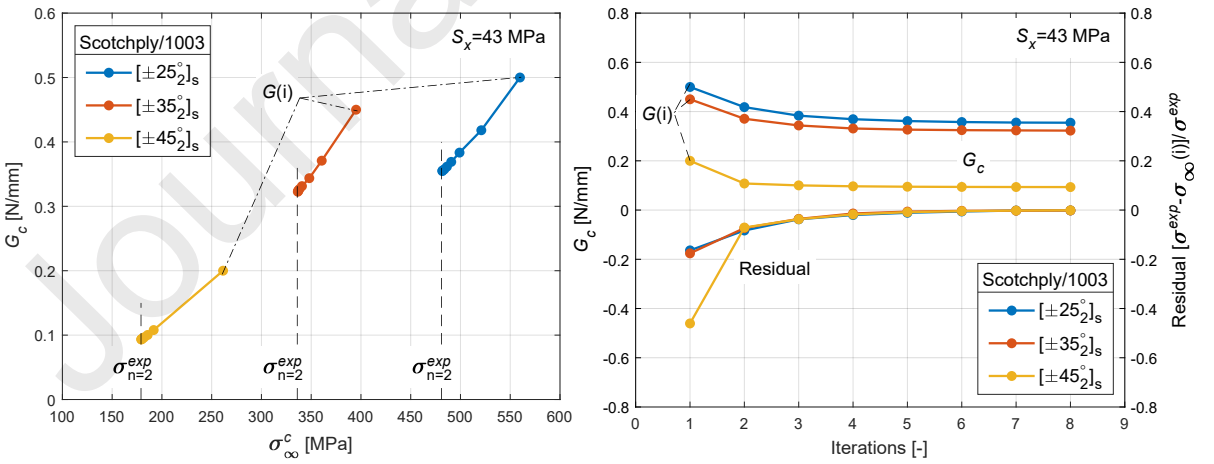

(a) (b)

Fig. 10. Evaluated interface fracture toughness for Scotchply/1003 laminate with respect to (a) experimental failure stress and (b) the corresponding number of iterations, across various ply orientations.

The calculated interface fracture toughness values for the considered laminates are presented in Fig. 11. In the case of M79/UD600, for fracture toughness validation purposes, a single toughness value is utilised for each orientation θ, encompassing varying normalised ply thicknesses n, to predict fracture stress under quasi-static loading conditions. The single toughness values, displayed in Table 3, are approximately the average toughness values of different ply thickness for each ply orientation. This prediction (by solving the 3D FFM static system ((1), (2))) is compared against experimental tests [65] and is presented in Fig. 12 (a). The corresponding normalised delamination onset width b^c/h is shown on the plot (right y-axis), illustrating a decreasing trend with increasing ply thickness.

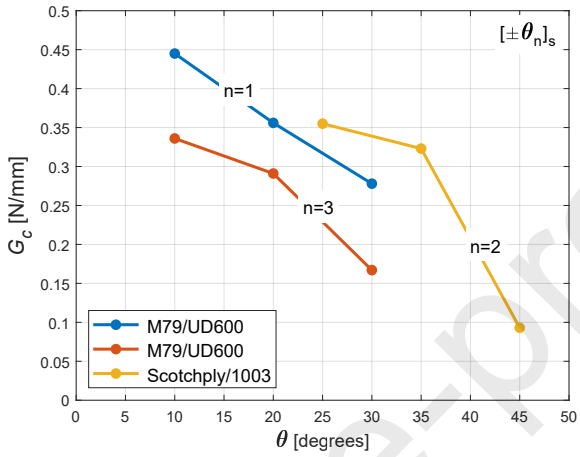

Fig. 11. The calculated interfacial fracture toughness for selected laminates versus ply orientation and norm. ply thickness.

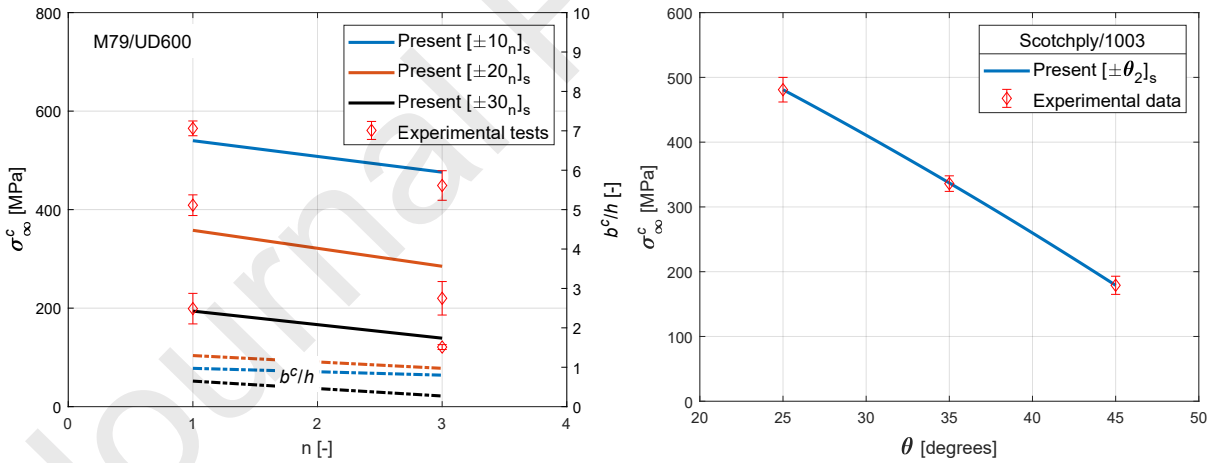

(a) (b)

Fig. 12. Prediction of failure stresses (solid lines) using 3D FFM static system (present) compared against experimental test results [65] (error bars) for (a) M79/UD600 at different ply orientations with its corresponding normalised crack width onset (right y-axis) relative to normalised ply thickness n, and (b) Scotchply/1003 with respect to ply orientation.

For Scotchply/1003, using the calculated toughness (Fig. 10 (a)), the predicted fracture stresses is shown in Fig. 12 (b) alongside experimental results [68]. Additionally, the obtained average delamination onset with, b^c_{av}, for Scotchply/1003 is 1.198 mm.

The determined fracture toughness values signify a noteworthy accuracy, in a sense that 3D FFM static criterion effectively predicts the reduction in failure stresses as ply thickness and ply orientation increase in the considered angle-ply laminates, aligning closely with experimental results. The calculated parameters (G_c, b_{av}^c) (Table 3) are utilised to evaluate interface properties in the fatigue regime (Section 2.3), which is discussed in the following section.

Table 3. Identified fracture toughness and average delamination onset width for selected laminates.

Material system	G_c (N/mm)						b_{av}^c (mm)
	10°	20°	25°	30°	35°	45°	
M79/UD600	0.37*	0.33*	-	0.2*	-	-	-
Scotchply/1003	-	-	0.355	-	0.323	0.093	1.198

*Approx. average of different ply thickness

3.3. Interfacial fracture parameters within the fatigue regime

The interface properties ($\sigma_{xz}^c(N)$, $\overline{G}_{max}(N)$) in the finite fatigue regime are evaluated using equations (11) and (13) for different nominal remote maximum stress cycle, σ_{max}^{∞}. Subsequently, material constants (l^s, m^s, l^g, m^g) are estimated using fitting interpolation procedure based on linear least squares. Calibration of (l^s, m^s) and (l^g, m^g) requires at least two points on the SN plot. In accordance with Ref. [57], two distinct methods are proposed to calibrate the critical distance for notches. The first method involves using only two extreme cases, i.e., static and fatigue limits. The second method utilises data on the SN plot spanning across a broad range of nominal stress amplitude to calibrate the critical distance. Due to data unavailability, the present investigation adopts the two-point data method. However, given the dispersion observed in the fatigue experimental data, it is recommended to incorporate additional data points to enhance fatigue estimation accuracy. It is noted here that incorporating a power law for the critical stress intensity factor (or equivalently ERR) in the fatigue regime as a function of number of cycles is equivalent to employing a power law for the critical distance [73]. Furthermore, based on fatigue experimental illustrations in Ref. [47] for $[\pm 45]_{2s}$ and Ref. [43] for ($[0/\pm 35/90]_s$, $[\pm 35/0/90]_s$, $[\pm 45/0/90]_s$), it is noted that stress/strain onset exhibits an approximately linear relationship as a function of the number of cycles in a log-log format within the range 10^2-10^6 cycles in laminates with free edge effect. Therefore, the current study adopts the assumption of a linear relationship in SN data in a log-log format within the range of 10^2-10^5 cycles for angle-ply laminates based on these observations, as the available experimental data used in the current study lies within this range.

It is noted here that only Scotchply/1003 laminate with $[\pm\theta_2]_s$ (where θ=25, 35, 45) is considered for fatigue investigation. The interface properties, $\sigma_{xz}^c(N)$ and $\overline{G}_{\max}(N)$, as a function of number of cycles for $[\pm 45_2]_s$ are shown in Fig. 13 (a) and (b), respectively. The

determined critical interlaminar shear stress at maximum nominal stress cycle σ_{xz}^{c} for $[\pm 45_2]_s$ is set constant for other $[\pm 25_2]_s$ and $[\pm 35_2]_s$ laminates. On the other hand, the critical incremental energy release rate at maximum nominal stress cycle, $\overline{G}_{max}$, for $[\pm 25_2]_s$ and $[\pm 35_2]_s$ are determined and shown in Fig. 14 (a) and (b), respectively. All the calibration curves are plotted in log-log format. The solid black lines represent best fitting curve using linear regression (Probability of Survival, P_s, 50%). The dashed red scatter bands represent a P_s of 97.7% and 2.3%. The calibrated material constants for all considered ply orientations are listed in Table 4.

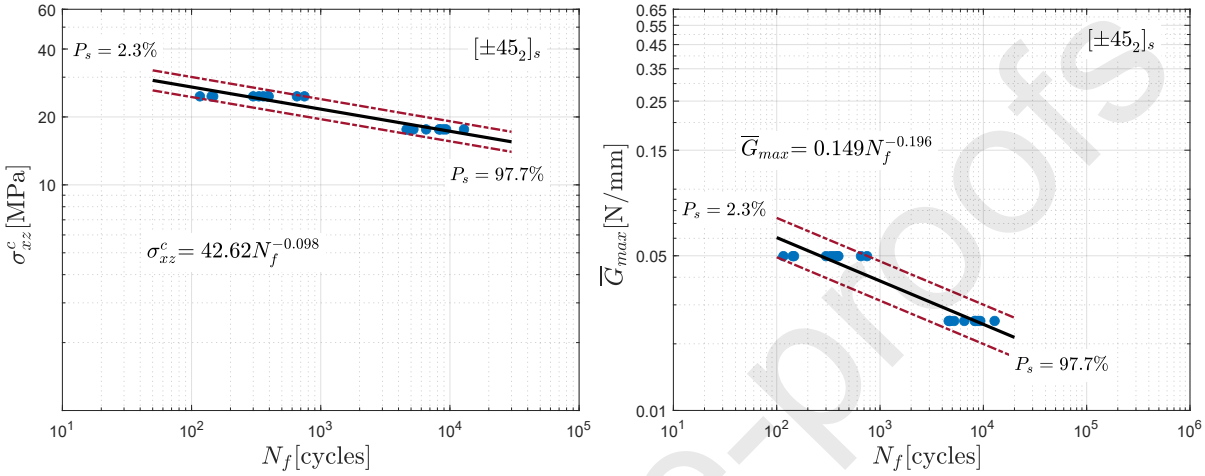

(a) (b)

Fig. 13. Calibration of fatigue curves for Scotchply/1003 for $[\pm 45_2]_s$: Critical (a) interlaminar shear stress and (b) incremental energy release rate, plotted at maximum nominal cyclic stress as a function of number of cycles. The dashed red lines represent a Probability of Survival (P_s) of 97.7% and 2.3%.

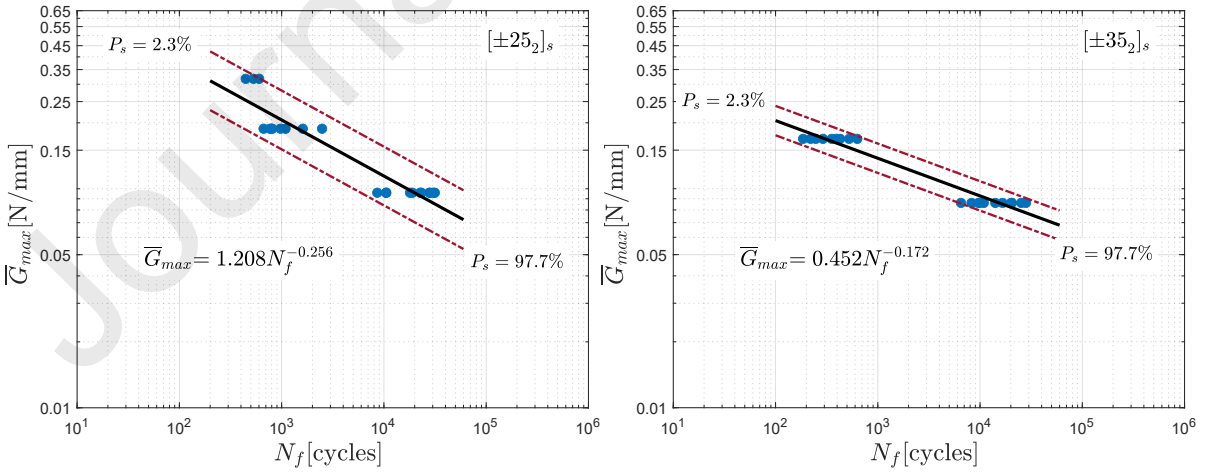

(a) (b)

Fig. 14. Calibration of fatigue curves for Scotchply/1003: Critical incremental energy release rate for (a) $[\pm 25_2]_s$ and (b) $[\pm 35_2]_s$, plotted at maximum nominal cyclic stress as a

function of number of cycles. The dashed red lines represent a Probability of Survival (P_s) of 97.7% and 2.3%.

Table 4. Determined material constants for different ply orientation.

	$\sigma_{xz}^{c}(N) = l^{s}\, N^{-m^{s}}$		$\overline{G}_{max}(N) = l^{g}\, N^{-m^{g}}$	
Layup				
	l^{s} [MPa]	m^{s}	l^{g} [N/mm]	m^{g}
$[\pm 25_2]_s$	42.62	0.098	1.208	0.256
$[\pm 35_2]_s$	42.62	0.098	0.452	0.172
$[\pm 45_2]_s$	42.62	0.098	0.149	0.196

3.4. Fatigue life assessment and 3D FFM model validation

This section validates the 3D FFM criterion within finite fatigue regime (Section 2.4) against the experimental test results taken from [68]. The experimental data corresponds to the free edge delamination of angle-ply laminates ($[\pm\theta_2]_s$ where θ=25, 35, 45) under tension-tension loading with a loading ratio of R=0.05. The experimental data serves as a benchmark for the random numerical predictions of number cycles to failure, N_f, which are obtained from the 3D FFM fatigue model for a given load ratio and nominal remote maximum stress cycle, σ_{max}^{∞}, after estimating the interface properties within the fatigue regime along with material constants (Section 3.3). The model's accuracy is assessed by comparing predicted finite fatigue lives against experimental values, using coefficient of determination, scatter bands, percentage error and prediction intervals. The validation demonstrates how the 3D FFM model captures the trends observed in experimental data, and any discrepancies are discussed.

The inequalities in Eq. (14) provide the number of cycles, N, needed by the stress and energy criteria for the initiation of a free edge delamination under fatigue loading, dependant on the homothetic crack dimensions a^{H} and b^{H}. These conditions are visually represented for the selected laminate in Fig. 15, demonstrating their reliance on a^{H} and b^{H}. This depiction emphasises the interaction between the respective surfaces, and the solution to system of equations (14) is achieved using a standard constrained nonlinear optimisation algorithm (discussed in Section 2.4). MATLAB's *fmincon* function is employed for the optimisation problem. The stress criterion indicates that smaller N values are associated with smaller b^{H} values for crack initiation. In contrast, according to energy criterion, N decreases as both crack

lengths increase, suggesting that larger cracks require smaller N for delamination onset. The surface that corresponds to energy criterion show wavy behaviour where one of the crack dimension a^{H} and b^{H} approaches to minimum (zero). This region is away from the interested zone where surfaces intersect. This may be due to the ERR sensitivity on the mesh near the semi-elliptical crack front when one of the crack dimensions approach minimum (zero). On the intersection curve of the two respective surfaces, the region with the minimum N values to failure corresponds to similar values of both delamination onset width and critical finite life. This indicates spontaneous delamination extension in a direction and the formation of long shallow cracks.

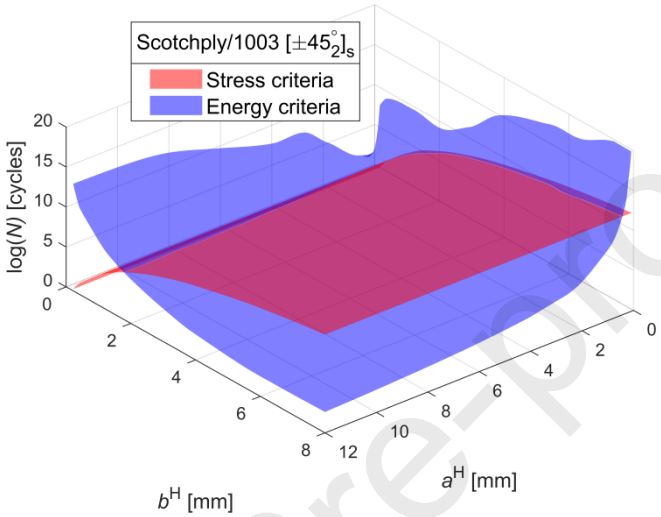

Fig. 15. Depiction of stress and energy conditions for the 3D FFM fatigue analysis: required N values for delamination onset based on homothetic crack lengths a^H and b^H, for $[\pm 45_2]_s$ stacking sequence of Scotchply/1003 material system.

The first example to predict the nominal stress-finite fatigue life of laminate with free edge effect using current 3D FFM fatigue criterion is of $[\pm 45_2]_s$ stacking sequence and is presented in Fig. 16. Fig. 17 (a) and (b) shows predictions for $[\pm 25_2]_s$ and $[\pm 35_2]_s$, respectively. The nominal remote maximum stress cycle, σ^{∞}_{max}, is plotted against number of cycles to failure, N_f. FFM finite fatigue model is in good agreement with the experiments except in $[\pm 35_2]_s$ configuration, model predictions are slightly unconservative. This deviation might be associated to the choice of interface property in fatigue regime, critical interlaminar maximum shear stress, taken for $[\pm 35_2]_s$. An appropriate choice of which can diminish this deviation. However, the deviation in prediction of finite fatigue life against experiments, considering the interface properties within fatigue regime, cannot be conclusively clarified. The finite delamination onset width, b^f, for $[\pm 45_2]_s$ is plotted on right y-axis in Fig. 16. The delamination onset illustrates decreasing trend against the number of cycles to failure.

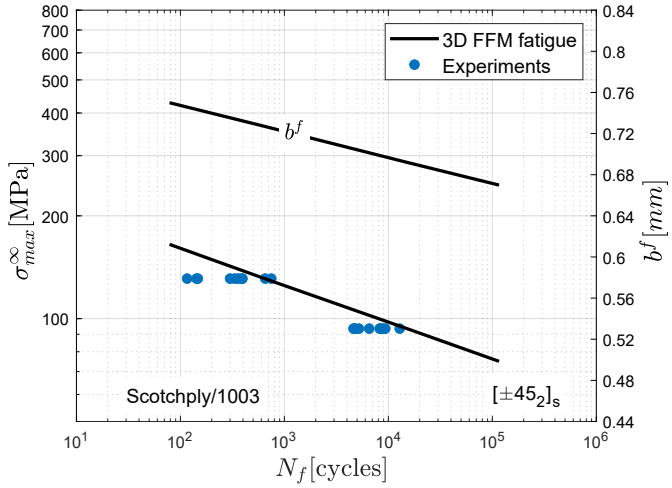

Fig. 16. Predicted finite fatigue life (solid line) compared against experimental test results [68] (blue markers) and corresponding normalised crack width onset (right y-axis) for Scotchply/1003 with $[\pm 45_2]_s$ stacking sequence.

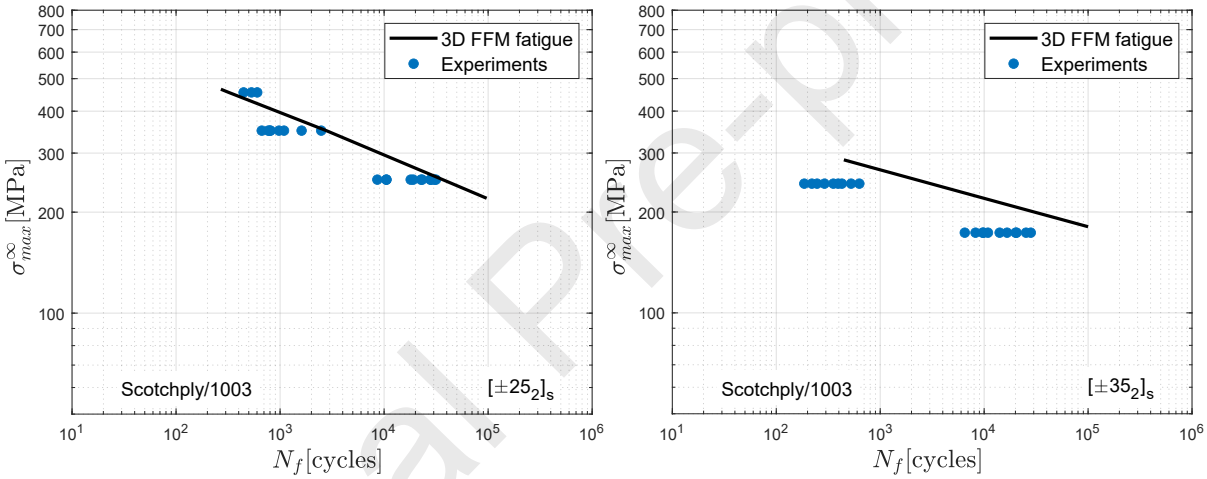

(a) (b)

Fig. 17. Predicted finite fatigue life (solid line) in comparison to experimental tests [68] (blue markers) for Scotchply/1003 with (a) $[\pm 25_2]_s$ and (b) $[\pm 35_2]_s$ stacking sequence.

To have a better assessment of 3D FFM fatigue criterion, Fig. 18 shows predictions of FFM estimations of finite fatigue life, N_f, of all configurations against the experiments, $N_{f,exp}$. The data above the solid black line refers to unconservative predictions. The predictions by FFM are comprised in ± 3 (red dashed) and ± 5 (black dashed) scatter bands. Furthermore, for the FFM fatigue model performance, coefficient of determination, R^2, is employed for the data that refers to the natural logarithm. Its value is 0.2479 with and 0.6761 without considering $[\pm 35_2]_s$ laminate. Additionally, the accuracy of the current 3D FFM fatigue criterion model is assessed using percentage error in log space for each stress range across all selected laminate configurations using:

$$\text{Percentage error (log space)} = \left|1 - \frac{\log_{10}(N_f)}{\left(\frac{1}{s}\sum_{i=1}^{s}\log_{10}(N_{f,exp,i})\right)}\right|\%, \quad (18)$$

where s represents the number of tested specimens for a given stress range for a selected laminate. Prediction interval 95% is also assessed in log space using:

$$\text{95\% Prediction interval (log space)} = \frac{1}{s}\sum_{i=1}^{s}\log_{10}(N_{f,exp,i}) \pm t_{dis}\ \text{std}(\log_{10}(N_{f,exp}))\sqrt{1+\frac{1}{s}}, \quad (19)$$

where t_{dis} is the t-multiplier from the t-distribution with degrees of freedom $s-1$, and std is the standard deviation calculated on the log-transformed experimental data.

Both Percentage error and prediction interval bounds have been tabulated in Table 5 for each stress range for all the selected laminate configurations. The prediction interval is calculated in log space as given by Eq.(19) and then converted back to the original scale (Table 5) for comparison with predicted finite fatigue life. All predictions are within the 95% prediction interval bounds except for the $[\pm 35_2]_s$ laminate at both 243 MPa and 173.5 MPa stress ranges, where the percentage error is notably higher at 37.8% and 25.68%, respectively, compared to the lower range of 6.55–14.08% observed for $[\pm 25_2]_s$ and $[\pm 45_2]_s$ configurations. As previously discussed, this deviation arises from the unconservative predictions of the 3D FFM model against experimental results for the $[\pm 35_2]_s$ laminate.

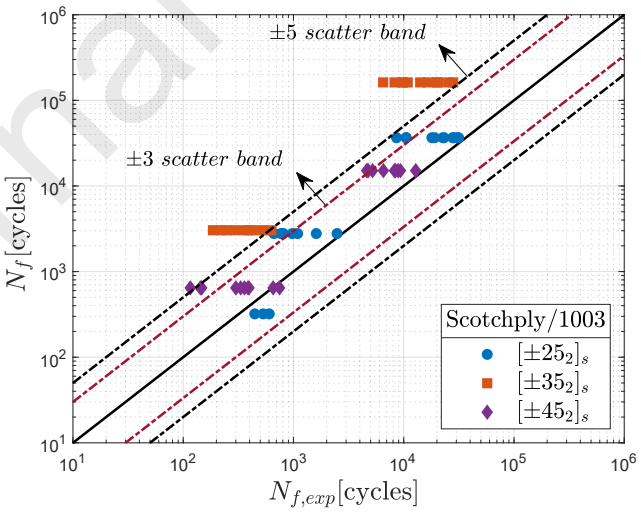

Fig. 18. 3D FFM fatigue model predictions for finite fatigue life of laminates exhibiting free edge effects against experimental tests. The ± 3 (red dashed) and ± 5 (black dashed) scatter bands are constructed around the 1:1 (solid black) line, representing factors of 3 and 5 of the model predictions.

Table 5. Accuracy values of current 3D FFM fatigue criterion against experimental data using percentage error and 95% prediction interval.

	Ply orientation						
	$[\pm 25_2]_s$			$[\pm 35_2]_s$		$[\pm 45_2]_s$	
Max stress (MPa)	455	350	250	243	173.5	131	93.5
Experiments $N_{f,exp}$ (cycles)	446 603 531	810 795 666 975 1091 769 1610 2485	10497 19050 28326 27815 8608 22650 30445 23213 10545 18003 31494	186 220 247 291 393 354 428 525 630	9862 8257 6511 9680 14094 16618 20095 20502 28106 25296 10877	116 143 147 332 300 359 748 387 654 395	4742 4618 4745 5214 6542 9336 8410 8245 8892 12851
3D FFM Prediction N_f (cycles)	321	2780	36600	3056	161472	645	15100
Percentage error (%)	7.81	14.08	6.55	37.8	25.68	13.23	8.77
95% Upper prediction interval (cycles)	1109	3178	56887	909	42818	1354	16143
95% lower prediction interval (cycles)	246	343	6472	126	4531	68	2990

Furthermore, the effects of ply orientation on finite fatigue life in laminates with free edge effect are studied. Fig. 19 (a) depicts that a higher nominal remote maximum stress cycle, σ_{max}^{∞}, is required for a laminate to fracture due to the free edge effect in lower angles of ply orientation, θ, to achieve the same fatigue life. However, for a given nominal remote maximum

stress cycle (percentage of static tensile strength, σ^{exp}), fatigue life decreases with increasing the ply orientation angle (Fig. 19 (b)). Fig. 19 (a) also reveals that decrease in σ^{∞}_{max} to increase fatigue life is more noticeable in lower θ than higher. It is important to note here that N_f of the $[\pm 35_2]_s$ configuration, as shown in Fig. 19 (b), exhibits a higher value compared to the anticipated decreasing trend. This deviation is due to an unconservative prediction in finite fatigue life, as seen in Fig. 17 (b). Typically, a decreasing trend can be expected when there is a good agreement in finite fatigue life predictions.

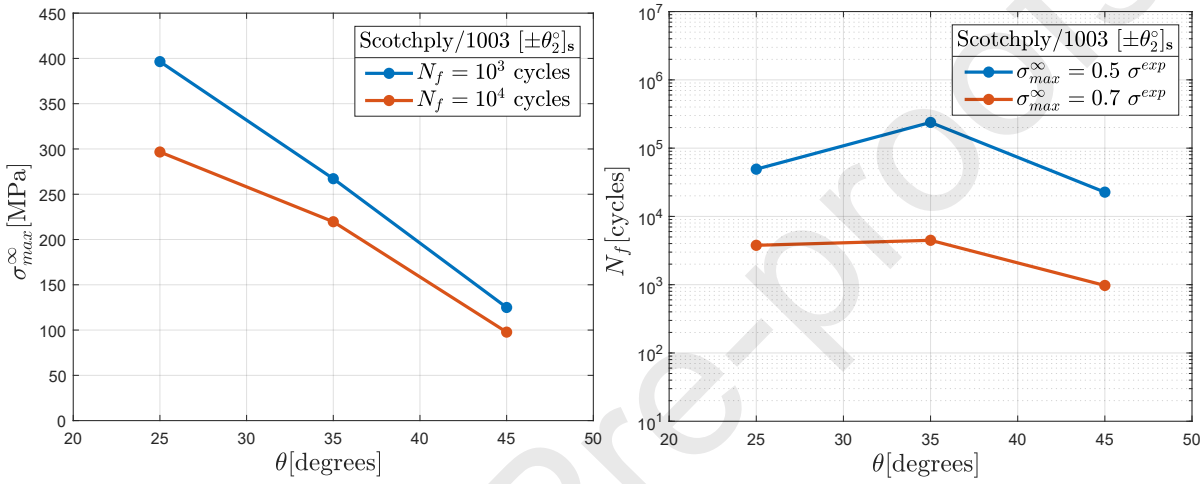

(a) (b)

Fig. 19. Influence of ply orientation on (a) nominal remote maximum stress cycle for a given finite fatigue lives, and (b) finite fatigue life for a given nominal remote maximum cycle stresses (percentages of static tensile strength, σ^{exp}) on a semi-log plot.

In lightweight structural design, such as in aerospace applications, stress concentrations such as free edge effect play a crucial role. Based on the current results, designers optimising laminate layups for improved fatigue resistance can consider lower ply orientation angles, as these can enhance fatigue life for a given nominal remote maximum stress cycle.

4. Conclusions

The 3D FFM model is proposed for prediction of fatigue life estimation of laminates exhibiting free edge effect. A 3D FFM fatigue criterion requires information of interface properties in fatigue regime, such as critical interlaminar stress and incremental energy release rate, as a function of number of cycles. For calibration of material constants, the critical stress is computed using effective interlaminar stress distribution in a certain length that is taken equal to average delamination onset width, while a quadratic relation is assumed between critical incremental energy release rate and nominal remote maximum stress cycle. The quantities like interlaminar stresses and incremental energy release rates are computed utilising expressions (obtained from dimensional analysis) and FE models. The 3D FFM criterion within fatigue regime also requires computation of fracture toughness and solution of static criterion for delamination onset width. Subsequently, the two inequalities of 3D FFM fatigue criterion is solved using non-linear constraint optimisation problem for a unique solution by assuming a

homothetic crack extension. The predictions of fatigue life estimation using proposed 3D FFM fatigue criterion is in general in good agreement with the experimental results from literature. The effects of ply orientation on finite fatigue life are also predicted. It is observed that lower angles of ply orientation in angle-ply laminates have higher fatigue life for a given remote cyclic load. The proposed 3D FFM fatigue criterion offers valuable insights into predicting delamination in laminates exhibiting free edge effects under fatigue loading. However, it requires a new numerical implementations at the interface for different composite layups, depending on which interface of the laminate triggers free edge delamination. This is because closed-form solutions for quantities such as interlaminar stresses and ERR may not be readily available for different stacking sequences. The applicability of the method relies on the accurate determination of these quantities for each specific composite configuration. Further work is needed to assess the reliability and accuracy of the proposed 3D FFM fatigue criterion, particularly regarding the incorporation of broader SN data for laminates exhibiting free edge effects.

CRediT authorship contribution statement

Mohammad Burhan: Conceptualisation, Methodology, Software, Validation, Formal Analysis, Investigation, Writing-Original Draft, Visualisation. Zahur Ullah: Writing - review and editing, Supervision, Project Administration, Funding acquisition. Zafer Kazancı: Writing - review and editing. Giuseppe Catalanotti: Writing - review and editing, Supervision, Funding acquisition.

Declaration of competing interest

The authors declare that they have no known competing financial interests or personal relationships that could have appeared to influence the work reported in this paper.

Data availability

Data will be made available on request.

Acknowledgements

This study was conducted as part of the Belfast Maritime Consortium UKRI Strength in Places project, 'Decarbonisation of Maritime Transportation: A return to Commercial Sailing' led by Artemis Technologies, Project no. 107138.

Appendix A

The outline to calculate G_c in laminates exhibiting free edge effects, considering prominent σ_{xz}, is as follows:

Step 1: Initialise G_c with random value, higher than the expected, $G_c(i)$.

Step 2: For a given static experimental failure stress σ^{exp}, and interlaminar shear strength S_x, solve numerically the system of equations:

$$\begin{cases} \dfrac{\pi ab}{2\int_{-a}^{a}\int_{0}^{b/a\sqrt{a^2-x^2}}\frac{\chi_{xz}}{S_x}\,dy\,dx} - \sigma^{exp} = R_1 \\ \sqrt{\dfrac{\pi ab\Im G_c(i)}{2h\int_{-a}^{a}\int_{0}^{b/a\sqrt{a^2-x^2}}(\psi_{II}{}^2+\psi_{III}{}^2)\,dy\,dx}} - \sigma^{exp} = R_2, \end{cases} \quad (20)$$

For a, and b while satisfying the condition of $\min(R_1^2 + R_2^2)$, where $R_1$and R_2 are residuals from the system of equations (1), respectively.

Step 3: Using calculated a and b in one of the equations (1) and solve numerically for $\sigma_\infty(i)$. Now use the calculated $\sigma_\infty(i)$ in updating $G_c(i)$ using:

$$G_c(i+1) = G_c(i)\left[1 + \left(\frac{\sigma^{exp} - \sigma_\infty(i)}{\sigma^{exp}}\right)\right], \quad (21)$$

with the condition $\sigma^{exp} \leq \sigma_\infty(i) < 2\sigma^{exp}$. In the instances if this condition is not satisfied, resulting in a $G_c(i+1)$ that is either negative, zero or greater than $G_c(i)$, it becomes imperative to adjust the initialised value $G_c(i)$ to ensure the validity of the subsequent iterations.

Step 4: Check whether the condition:

$$G_c(i+1) \cong G_c(i)\,, \quad (22)$$

is satisfied, in that case $G_c(i+1)$ is the interface toughness, otherwise go to step 2 with the next iteration and repeat the process until convergence is achieved.

References

[1] Hayashi T. Analytical Study of Interlaminar Shear Stresses in Laminated Composite Plate. Trans Jpn Soc Aeronaut Sp. Sci, 1967, p. 43–8.

[2] Mittelstedt C, Becker W, Kappel A, Kharghani N. Free-Edge Effects in Composite Laminates-A Review of Recent Developments 2005-2020. Appl Mech Rev 2022;74:1–18. https://doi.org/10.1115/1.4054145.

[3] Pipes RB, Pagano NJ. Interlaminar Stresses in Composite Laminates Under Uniform Axial Extension. J Compos Mater 1970;4:538–48. https://doi.org/10.1177/002199837000400409.

[4] Mittelstedt C, Becker W. Semi-analytical computation of 3D stress singularities in linear elasticity. Commun Numer Methods Eng 2005;21:247–57. https://doi.org/10.1002/cnm.742.

[5] Dölling S, Hahn J, Felger J, Bremm S, Becker W. A scaled boundary finite element method model for interlaminar failure in composite laminates. Compos Struct 2020;241:111865. https://doi.org/10.1016/j.compstruct.2020.111865.

[6] Pagano NJ, Pipes RB. The Influence of Stacking Sequence on Laminate Strength. J Compos Mater 1971;5:50–7. https://doi.org/10.1007/978-94-017-2233-9_20.

[7] Pagano NJ, Pipes RB. Some observations on the interlaminar strength of composite laminates. Int J Mech Sci 1973;15. https://doi.org/10.1016/0020-7403(73)90099-4.

[8] Kassapoglou C, Lagace PA. Closed Form Solutions for the Interlaminar Stress Field in Angle-Ply and Cross-Ply Laminates. J Compos Mater 1987;21:292–308. https://doi.org/10.1177/002199838702100401.

[9] Wang SS, Choi I. Boundary-layer effects in composite laminates: Part 1 free-edge stress singularities. J Appl Mech Trans ASME 1982;49:541–8. https://doi.org/10.1115/1.3162514.

[10] Wang SS, Choi I. Boundary-Layer Effects in Composite Laminates-Part 2. J Appl Mech 1982;49:541–8.

[11] Mittelstedt C, Becker W. The Pipes-Pagano-problem revisited: Elastic fields in boundary layers of plane laminated specimens under combined thermomechanical load. Compos Struct 2007;80:373–95. https://doi.org/10.1016/j.compstruct.2006.05.018.

[12] Yao WA, Nie YZ, Xiao F. Analytical solutions to edge effect of composite laminates based on symplectic dual system. Appl Math Mech (English Ed 2011;32:1091–100. https://doi.org/10.1007/s10483-011-1483-7.

[13] Nosier A, Maleki M. Free-edge stresses in general composite laminates. Int J Mech Sci 2008;50:1435–47. https://doi.org/10.1016/j.ijmecsci.2008.09.002.

[14] Sarvestani HY, Sarvestani MY. Free-edge stress analysis of general composite laminates under extension, torsion and bending. Appl Math Model 2012;36:1570–88. https://doi.org/10.1016/j.apm.2011.09.028.

[15] Yazdani Sarvestani H, Yazdani Sarvestani M. Interlaminar stress analysis of general composite laminates. Int J Mech Sci 2011;53:958–67. https://doi.org/10.1016/j.ijmecsci.2011.07.007.

[16] Islam MS, Prabhakar P. Modeling framework for free edge effects in laminates under thermo-mechanical loading. Compos Part B Eng 2017;116:89–98. https://doi.org/10.1016/j.compositesb.2017.01.072.

[17] Raju IS, Crews JH. Interlaminar stress singularities at a straight free edge in composite laminates. Comput Struct 1981;14:21–8.

[18] Ye L, Yang BX. Boundary Layer Approach To Interlaminar Stresses in Composite Laminates With Curved Edges. J Reinf Plast Compos 1988;7:179–98. https://doi.org/10.1177/073168448800700207.

[19] Salamon NJ. An Assessment of the Interlaminar Stress Problem in Laminated Composites. J Compos Mater 1980;14:177–94. https://doi.org/10.1177/002199838001400114.

[20] Kant T, Swaminathan K. Estimation of transverse/interlaminar stresses in laminated composites - a selective review and survey of current developments. Compos Struct 2000;49:65–75. https://doi.org/10.1016/S0263-8223(99)00126-9.

[21] Mittelstedt C, Becker W. Free-edge effects in composite laminates. Appl Mech Rev 2007;60:217–45. https://doi.org/10.1115/1.2777169.

[22] Zhou S, Sun CT. Failure Analysis of Composite Laminates with Free Edge. J Compos Technol \& Res 1990;12:91–7.

[23] Kim RY, Soni SR. Experimental and Analytical Studies On the Onset of Delamination in Laminated Composites. J Compos Mater 1984;18:70–80. https://doi.org/10.1177/002199838401800106.

[24] Lagunegrand L, Lorriot T, Harry R, Wargnier H, Quenisset JM. Initiation of free-edge delamination in composite laminates. Compos Sci Technol 2006;66:1315–27. https://doi.org/10.1016/j.compscitech.2005.10.010.

[25] Brewer JC, Lagace PA. Quadratic Stress Criterion for Initiation of Delamination. J Compos Mater 1988;22:1141–55. https://doi.org/10.1177/002199838802201205.

[26] Whitney JM., Nuismer RJ. Stress Fracture Criteria for Laminated Composites Containing Stress Concentrations. J Compos Mater 1974;8:253–65.

[27] Wang A, Crossman FW. Initiation and Growth of Transverse Cracks and Edge Delamination in Composite Laminates Part 1. An Energy Method. J Compos Mater 1980;14:71–87.

[28] Leguillon D. A method based on singularity theory to predict edge delamination of laminates. Int J Fract 1999;100:105–20.

[29] O'Brien TK. Characterization of Delamination Onset and Growth in a Composite Laminate. Damage Compos Mater ASTM STP 775, KL Reifsnider, E.d, Am Soc Test Mater 1982:140–67. https://doi.org/10.1520/STP34325S.

[30] Taylor D. The theory of critical distances. Eng Fract Mech 2008;75:1696–705. https://doi.org/10.1016/j.engfracmech.2007.04.007.

[31] Leguillon D. Strength or toughness? A criterion for crack onset at a notch. Eur J Mech A/Solids 2002;21:61–72. https://doi.org/10.1016/S0997-7538(01)01184-6.

[32] Weißgraeber P, Leguillon D, Becker W. A review of Finite Fracture Mechanics: crack initiation at singular and non-singular stress raisers. Arch Appl Mech 2016;86:375–401. https://doi.org/10.1007/s00419-015-1091-7.

[33] Doitrand A, Duminy T, Girard H, Chen X. A review of the coupled criterion. Hal-04023438 2023.

[34] Burhan M, Ullah Z, Kazancı Z, Catalanotti G. A critical review on free edge delamination fracture criteria. Mech Adv Mater Struct 2024:1–14. https://doi.org/10.1080/15376494.2024.2424492.

[35] Leguillon D. An attempt to extend the 2D coupled criterion for crack nucleation in brittle materials to the 3D case. Theor Appl Fract Mech 2014;74:7–17. https://doi.org/10.1016/j.tafmec.2014.05.004.

[36] García IG, Carter BJ, Ingraffea AR, Mantič V. A numerical study of transverse cracking in cross-ply laminates by 3D finite fracture mechanics. Compos Part B Eng 2016;95:475–87. https://doi.org/10.1016/j.compositesb.2016.03.023.

[37] Doitrand A, Fagiano C, Carrère N, Chiaruttini V, Hirsekorn M. Damage onset modeling in woven composites based on a coupled stress and energy criterion. Eng Fract Mech 2017;169:189–200. https://doi.org/10.1016/j.engfracmech.2016.11.021.

[38] Doitrand A, Leguillon D. 3D application of the coupled criterion to crack initiation prediction in epoxy/aluminum specimens under four point bending. Int J Solids Struct 2018;143:175–82. https://doi.org/10.1016/j.ijsolstr.2018.03.005.

[39] Doitrand A, Leguillon D. Comparison between 2D and 3D applications of the coupled criterion to crack initiation prediction in scarf adhesive joints. Int J Adhes Adhes 2018;85:69–76. https://doi.org/10.1016/j.ijadhadh.2018.05.022.

[40] Hebel J, Dieringer R, Becker W. Modelling brittle crack formation at geometrical and material discontinuities using a finite fracture mechanics approach. Eng Fract Mech 2010;77:3558–72. https://doi.org/10.1016/j.engfracmech.2010.07.005.

[41] Martin E, Leguillon D, Carrère N. A twofold strength and toughness criterion for the onset of free-edge shear delamination in angle-ply laminates. Int J Solids Struct 2010;47:1297–305. https://doi.org/10.1016/j.ijsolstr.2010.01.018.

[42] Frey C, Dölling S, Becker W. Closed-form analysis of interlaminar crack initiation in angle-ply laminates. Compos Struct 2021;257:113060. https://doi.org/10.1016/j.compstruct.2020.113060.

[43] O'Brien TK. Mixed-mode strain-energy-release rate effects on ede delamination of composites. Eff Defects Compos Mater ASTM STP 836, Am Soc Test Mater 1984:125–42.

[44] O'Brien TK. Fatigue Delamination Behavior of PEEK Thermoplastic Composite Laminates. J Reinf Plast Compos 1988;7:341–59. https://doi.org/10.1177/073168448800700403.

[45] O'Brien TK. Local delamination in laminates with angle ply matrix cracks, part II: delamination fracture analysis and fatigue characterization. Compos Mater Fatigue Fract Fourth Vol ASTM STP 1156, WW Stinchcomb NE Ashbaugh, Eds, Am Soc Test Mater Philadelphia 1993:507–38. https://doi.org/10.1520/stp24748s.

[46] Scarponi C, Barboni R. Delaminations onset and propagation for CFRP angle ply laminates under uniaxial fatigue loads. J Reinf Plast Compos 1997;16:1181–95.

[47] Kim RY, Crasto AS. Initiation of Free-Edge Delamination in a Composite Laminate Under Fatigue Loading. Proc. ICCM-11, Gold Coast, Aust. July, 1997.

[48] Papanikos P, Tserpes KI, Pantelakis S. Modelling of fatigue damage progression and life of CFRP laminates. Fatigue Fract Eng Mater Struct 2003;26:37–47. https://doi.org/10.1046/j.1460-2695.2003.00585.x.

[49] Lorriot T, Marion G, Harry R, Wargnier H. Onset of free-edge delamination in composite laminates under tensile loading. Compos Part B Eng 2003;34:459–71. https://doi.org/10.1016/S1359-8368(03)00016-7.

[50] Lagace P, Brewer J, Kassapoglou C. Effect of Thickness on Interlaminar Stresses and Delamination in Straight-Edged Laminates. J Compos Technol Res 1987;9:81–7. https://doi.org/10.1520/ctr10246j.

[51] Burhan M, Scalici T, Ullah Z, Kazancı Z, Catalanotti G. A three-dimensional Finite Fracture Mechanics model to predict free edge delamination in angle ply laminates. Eng Fract Mech 2024;306:110156. https://doi.org/10.1016/j.engfracmech.2024.110156.

[52] Tsai SW, Melo JDD. An invariant-based theory of composites. Compos Sci Technol 2014;100:237–43. https://doi.org/10.1016/j.compscitech.2014.06.017.

[53] Sapora A, Cornetti P, Campagnolo A, Meneghetti G. Fatigue limit: Crack and notch sensitivity by Finite Fracture Mechanics. Theor Appl Fract Mech 2020;105:102407. https://doi.org/10.1016/j.tafmec.2019.102407.

[54] Sapora A, Cornetti P, Campagnolo A, Meneghetti G. Mode I fatigue limit of notched structures: A deeper insight into Finite Fracture Mechanics. Int J Fract 2021;227:1–13. https://doi.org/10.1007/s10704-020-00488-6.

[55] Mirzaei AM, Cornetti P, Sapora A. A novel Finite Fracture Mechanics approach to assess the lifetime of notched components. Int J Fatigue 2023;173:107659. https://doi.org/10.1016/j.ijfatigue.2023.107659.

[56] Krueger R. Development and application of benchmark examples for mode II static delamination propagation and fatigue growth predictions. No NASA/CR–2011-217305 2011.

[57] Susmel L, Taylor D. A novel formulation of the theory of critical distances to estimate lifetime of notched components in the medium-cycle fatigue regime. Fatigue Fract Eng Mater Struct 2007;30:567–81. https://doi.org/10.1111/j.1460-2695.2007.01122.x.

[58] Donaldson SL. Mode III interlaminar fracture characterization of composite materials. Compos Sci Technol 1988;32:225–49. https://doi.org/10.1016/0266-3538(88)90022-X.

[59] Liao WC, Sun CT. The determination of Mode III fracture toughness in thick composite laminates. Compos Sci Technol 1996;56:489–99. https://doi.org/10.1016/0266-3538(96)00009-7.

[60] Beber VC, Fernandes PHE, Schneider B, Brede M, Mayer B. Fatigue lifetime

prediction of adhesively bonded joints: An investigation of the influence of material model and multiaxiality. Int J Adhes Adhes 2017;78:240–7. https://doi.org/10.1016/j.ijadhadh.2017.08.007.

[61] Neuber H. Theory of notch stresses : principles for exact calculation of strength with reference to structural form and material, 1958.

[62] Sun CT, Zhou SG. Failure of Quasi-Isotropic Composite Laminates with Free Edges. J Reinf Plast Compos 1988;7:515–57. https://doi.org/10.1177/073168448800700602.

[63] Burhan M, Scalici T, Ullah Z, Kazancı Z, Catalanotti G. Investigating factors influencing interlaminar stresses and energy release rates of semi-elliptical cracks at free edges. Eng Fract Mech 2024:110274.

[64] Krueger R. Virtual crack closure technique: History, approach, and applications. Appl Mech Rev 2004;57:109–43. https://doi.org/10.1115/1.1595677.

[65] Burhan M, Sands C, McCreight T, Ullah Z. Effects of ply hybridisation on delamination in hybrid laminates at CorTen steel/M79LT-UD600 composite interfaces. UK Assoc. Comput. Mech. Conf. 2024 - Coombs, 2024. https://doi.org/10.62512/conf.ukacm2024.040.

[66] Hexcel Composites. Hexcel M79: Low Temperature Curing Epoxy Matrix, Product Data. Publication FTU302. 2014. https://www.mikecompositi.it/images/file/DS-MSDS/Resine/M79_eu_DS.PDF.

[67] Burhan M, Ullah Z. Experimental and numerical investigation of fracture characteristics in hybrid steel/composite and monolithic angle-ply laminates. SSRN Prepr 2024. https://doi.org/10.2139/ssrn.4838504.

[68] Kujawski D. Width effects on the tensile strength and fatigue behavior of angle-ply laminates. Int J Fatigue 1998;20:575–80. https://doi.org/10.1016/S0142-1123(98)00033-4.

[69] Im J, Mandell JF, Wang S, McGarry F. Surface crack growth in fiber composites. (No NASA-CR-135094) 1976.

[70] Hoover JW. Transverse cracking of [±θ/90_3]s composite laminates. MSc Thesis, Department of Mechanical Engineering, University of Alberta, 1999.

[71] Laffan MJ, Pinho ST, Robinson P, Iannucci L. Measurement of the in situ ply fracture toughness associated with mode I fibre tensile failure in FRP. Part II: Size and lay-up effects. Compos Sci Technol 2010;70:614–21. https://doi.org/10.1016/j.compscitech.2009.12.011.

[72] Harris CE, Morris DH. Fracture behaviour of thick, laminated graphite/epoxy composites. NASA Contract Rep 3784; 1984.

[73] Mirzaei AM, Mirzaei AH, Shokrieh MM, Sapora A, Cornetti P. Fatigue life assessment of notched laminated composites: Experiments and modelling by Finite Fracture Mechanics. Compos Sci Technol 2024;246:110376. https://doi.org/10.1016/j.compscitech.2023.110376.

Declaration of interests

1. Declaration of interests

☒ The authors declare that they have no known competing financial interests or personal relationships that could have appeared to influence the work reported in this paper.

☐The authors declare the following financial interests/personal relationships which may be considered as potential competing interests:

2. Contributions

☒ Each author declares substantial contributions through the following:

(1) the conception and design of the study, or acquisition of data, or analysis and interpretation of data, (2) drafting the article or revising it critically for important intellectual content,

Please indicate for each author the author contributions in the text field below. Signatures are not required.

Mohammad Burhan: Conceptualization, Methodology, Software, Validation, Formal Analysis, Investigation, Writing-Original Draft, Visualization. Zahur Ullah: Writing - review and editing, Supervision, Project Administration, Funding acquisition. Zafer Kazancı: Writing - review and editing. Giuseppe Catalanotti: Writing - review and editing, Supervision, Funding acquisition.

3. Approval of the submitted version of the manuscript

☒ Please check this box to confirm that all co-authors have read and approved the version of the manuscript that is submitted. Signatures are not required.

Declaration of interests

1. Declaration of interests

☒ The authors declare that they have no known competing financial interests or personal relationships that could have appeared to influence the work reported in this paper.

☐The authors declare the following financial interests/personal relationships which may be considered as potential competing interests:

2. Contributions

☒ Each author declares substantial contributions through the following:

(1) the conception and design of the study, or acquisition of data, or analysis and interpretation of data, (2) drafting the article or revising it critically for important intellectual content,

Please indicate for each author the author contributions in the text field below. Signatures are not required.

Mohammad Burhan: Conceptualization, Methodology, Software, Validation, Formal Analysis, Investigation, Writing-Original Draft, Visualization. Zahur Ullah: Writing - review and editing, Supervision, Project Administration, Funding acquisition. Zafer Kazancı: Writing - review and editing. Giuseppe Catalanotti: Writing - review and editing, Supervision, Funding acquisition.

3. Approval of the submitted version of the manuscript

☒ Please check this box to confirm that all co-authors have read and approved the version of the manuscript that is submitted. Signatures are not required.